ELSEVIER

Contents lists available at ScienceDirect

Computers and Electronics in Agriculture

journal homepage: www.elsevier.com/locate/compag





A drought stress-sensing technique based on wavelet entropy of chlorophyll fluorescence excited with pseudo-random binary sequence

Qian Xia^a, Hao Tang^a, Lijiang Fu^a, Jinglu Tan^b, Ya Guo^{a,*}

- ^a Key Laboratory of Advanced Process Control for Light Industry, Ministry of Education, Jiangnan University, Wuxi 214122, China
- b Department of Biomedical, Biological & Chemical Engineering, University of Missouri, Columbia, MO 65211, USA

ARTICLE INFO

Keywords:
Drought stress
Chlorophyll a fluorescence
Wavelet analysis
Photosynthesis

ABSTRACT

Drought stress is one of the most important environmental factors limiting photosynthesis and agriculture yield, but photosynthesis-based drought stress measures are still not well developed. Chlorophyll a fluorescence (ChlF) from photosynthesis II (PSII) tightly couples with photosynthesis and may potentially serve as a measure of drought stress. Traditional ChlF measurement is usually based on a step or pulse excitation, and may not perturb the complex photochemical reactions to show strong ChlF difference under drought stress conditions and limit the sensitivity and robustness of using ChlF to sense drought stress. In this work, a drought stress-sensing technique based on ChlF excited by pseudo-random binary sequence (PRBS) and analyzed by wavelet entropy was established. Four different rice (Oryza sativa L.) varieties with 120 samples for each variety and thirty spinach (Spinacia oleracea L.) samples were measured under different drought stress durations to validate the proposed method. Results show that the proposed wavelet-entropy-based ChlF measure could differentiate all the different drought stress durations for all rice varieties and spinach but the commonly used OJIP-based ChlF induction analysis could not. This work provides a new plant-physiology-based drought stress measurement method and ChlF analysis technique.

1. Introduction

The world population may reach 9.6 billion by 2050 and 10.9 billion by 2100 (Gerland et al., 2014). Demand for food will continue to increase. It is reported that reduction of precipitation and intensification of greenhouse effect will inevitably cause more extreme and severe weather events (Webber et al., 2018), which will reduce agricultural productivity. Drought is one of the major stresses that limit crop yield and has become a word-wide research focus (Barnabás et al., 2008; Liu et al., 2018; Dietz et al., 2021).

In photosynthesis, antenna chlorophyll molecules in photosystem II (PSII) jump from the ground state to a high-energy state after absorbing light energy. Chlorophyll molecules in the high-energy state are unstable and will return the ground state by releasing the absorbed light energy through heat, chlorophyll fluorescence (ChIF), or photochemical reactions (Lubitz et al., 2008; Kalaji et al., 2014; Ruban, 2016). The three energy dissipation pathways compete with one another, which makes ChIF useful in reflecting changes in photosynthesis (Murchie and Lawson, 2013; Esmaeilizadeh et al., 2021). At present, there are different methods for measurement of plant stresses including

reflectance indices (Sukhova and Sukhov, 2019; Sukhova et al., 2021; Sukhova et al., 2022a; Sukhova et al., 2022b), and hyperspectral imaging techniques (Mahlein et al., 2018); however, they are not like ChlF measurement, which is fully coupled with photosynthetic electron transport process (Gameiroa et al., 2016). ChlF thus has been extensively used in photosynthesis research (Murchie et al., 2013; Krause and Weis, 1991; Mohammed et al., 2019; Wangpraseurt et al., 2019; Dabrowski et al., 2021; Gorbunov and Falkowski, 2022; He et al., 2022), including drought stress measurement (Mathobo et al., 2017; Banks, 2018; Yao et al., 2018; Dabrowski et al., 2019; Xia et al., 2022). Moreover, research on plant phenotypes has become increasingly important in plant research and applications (Fiorani and Schurr, 2013). Structural and photosynthetic parameters are keys to phenotype characterizations (Simon et al., 2013; Cruz et al., 2016). As an optical method, ChlF technology is important in measuring photosynthetic parameters for plant phenotyping.

Photosynthetic activities involve many chemical reaction processes with a large span of reaction rates, which make the system a high-order system with broadband dynamics. In traditional ChIF measurement, leaves are often illuminated by light with a step or pulse signal (Guo and Tan, 2015). According to system and control theories (Wang et al., 2019;

E-mail addresses: tanj@missouri.edu (J. Tan), guoy@jiangnan.edu.cn (Y. Guo).

^{*} Corresponding author.

Abbreviations

OJIP Parameters Definition

Vi = (Fi - Fo)/(Fm - Fo) Relative variable fluorescence intensity at the I step

Vj = (Fj - Fo)/(Fm - Fo) Relative variable fluorescence intensity at the J step

Fv/Fo = (Fm - Fo)/Fo Quantum efficiency of photosystem II

Fm/Fo Electron transport through photosystem II

Fv/Fm = (Fm - Fo)/Fm Maximum photochemical quantum yield of photosystem II in the dark

Ss The smallest Sm turn-over (single turn-over)

Mo = $4\times(F300$ -Fo)/(Fm -Fo) Approximated initial slope (in ms-1) of the fluorescence transient

 $\phi Eo = (1 \text{ - (Fo/Fm)} \times (Fv/Fm) \;\; Quantum \ yield \ of \ electron \\ transport$

 $\phi Po = 1$ - (Fo/Fm)(or Fv/Fm) Maximum quantum yield of PSII

 $\phi Do = 1 - \phi Po - (Fo/Fm)$ Quantum yield of energy dissipation

 $\psi o = 1$ - Vj $\,$ Probability that a trapped exciton moves an electron further than OA-

ABS/RC = (Mo/Vj)(1/ ϕ Po) Absorption per reaction center PI_{ABS}=4[(F300-Fo)×(Fm-Fj) ×Fm]/[(Fm - Fo)(Fj - Fo)×Fo] Performance index for energy conservation from exciton to the reduction of Intersystem electron acceptors

ETo/RC=(Mo/Vj)(1-Vj) Electron transport per reaction center TRo/RC = Mo \times (1/Vj) Trapped energy flux per reaction center DIo/RC=ABS/RC-TRo/RC Dissipation per reaction center (at t = 0)

Sun et al., 2020; Chen et al., 2022), the frequency band of a step or a pulse excitation is narrow and may not perturb the system to produce rich reaction differences associated with stresses as a broadband excitation does. Broadband excitations can stimulate more dynamic characteristics of systems (Pan and Dai, 2018; Zhang et al., 2019). This may explain the controversial results from using ChIF to sense drought stress through the traditional ChIF induction measurement in the literature (Guo and Tan, 2015a).

When plants are stressed, various photochemical reaction coefficients and substance concentrations in the PSII may change (Wols and Hofman-Caris, 2012), which will affect the time-frequency dynamic characteristics of the system, and change the complexity of ChIF signals in both the time and frequency domains. This implies that the richness of the ChIF variations can be used for drought stress level differentiation. At present, ChIF parameters from traditional excitation signals can show

differences between control and stressed groups, but it is difficult to sense differences among different stress levels (Zhuang et al., 2020). Please refer to Tsimilli-Michael (2020) for the concepts, assumptions, definitions, and terms for more ChlF parameters. Information entropy is a measure of signal uncertainty and is often used to characterize signal complexity. The more uncertain, the more complex the signal, the greater its entropy (Qu et al., 2003; Wang et al., 2021). However, in the literature, there is a void of using ChlF information entropy for sensing.

In sum, there is a need to perturb the photosynthetic systems more persistently with a broadband excitation and analyze the entropy of complex ChlF responses for drought stress measurement. In this work, a broadband-based ChlF measure for drought stress and a new framework for analyzing ChlF signal in terms of entropy were proposed. Broadband excitation signals include white noise, PRBS, swept sine. PRBS is a binary sequence that can be designed, repeatedly generated and replicated. In addition, a PRBS signal is easy to implement with a circuit, and has a wide range of applications as an excitation source. Therefore, a PRBS signal as the broadband signal was used to stimulate ChlF in this work. Wavelet analysis, a powerful time-frequency analysis method, was used to decompose the ChlF signal into different frequency bands. The information entropy of the decomposed signal in different bands were computed to characterize drought-induced ChlF changes and a drought stress sensing technique based on PRBS-excited ChlF and wavelet entropy was established accordingly. It is expected that the proposed method for ChlF analysis will improve drought stress sensing upon the traditional ChlF analysis methods. Experiments were used to validate the developed method.

2. Method

2.1. Wavelet transform

Wavelet transform (WT) is a time-frequency localized signal analysis method (Akujuobi, 2022; Guido, 2022), which is suitable for analyzing time-varying signals with a broad band. WT adopts large time window for low frequency components and small time window for high frequency components, which make it have good time-frequency analysis capability with multi-scale detailed analysis of signals through the operation functions of scaling and translation. WT can be classified into continuous wavelet transform (CWT) and discrete wavelet transform (DWT). DWT is the discretization of the former (Sundararajan, 2016). In practical applications, CWT is associated with a large amount of calculation and high coefficient redundancy, so DWT is used in this work. The wavelet basis functions are generated by using parameters a, b, and a mother wavelet $\psi(t)$, where $\psi(t) \in L^2(R)$ ($L^2(R)$) is space of functions). The wavelet basis function $\psi_{a,b}(t)$ can be expressed as:

$$\Psi_{a,b}(t) = |a|^{-1/2} \times \Psi((t-b)/a) \quad a, b \in R, a > 0$$
 (1)

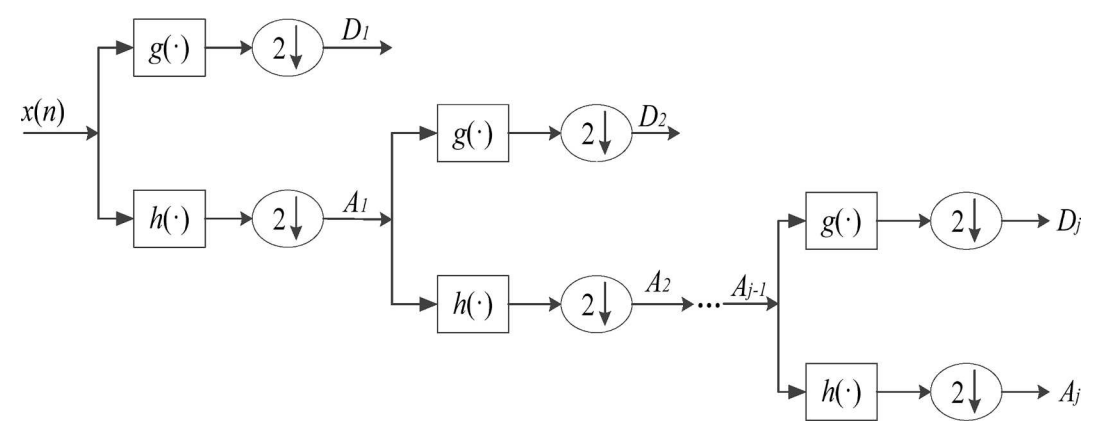


Fig. 1. Discrete wavelet decomposition.

where a is the scale parameter (scaling factor), which represents the resolution of the signal being processed and corresponds to the frequency domain analysis; b is the displacement parameter (translation factor), which corresponds to the time domain analysis; t is the independent variable of wavelet basis function and is the time variable in this work.

DWT realizes WT by using the discretization of wavelet scale and some translation rules. In order not to lose information, binary sampling is used to discretize a and b. Let $a=2^j, b=2^jk$, j and $k \in \mathbb{Z}$. The discrete wavelet function family obtained by $\psi_{a,b}(t)$ discretization is:

$$\Psi_{i,k}(t) = 2^{-j/2} \times \Psi(2^{-j}t - k) \tag{2}$$

where j is the scale parameter and k is the translation parameter. Daubechies wavelets have been successfully used in many applications (Özbay et al., 2011, Guo et al., 2015b), and Daubechies 4 (db4) was used as the wavelet basis function in this work.

DWT of the ChlF signal uses a high pass filter, a low pass filter, and two down-samplers. The high pass filter $g(\cdot)$ is the discrete mother wavelet and the low pass filter $h(\cdot)$ is its mirror version. The discrete ChlF signal x(n) is rapidly transformed at the instant k and scale j, and the output results of the high pass filter $g(\cdot)$ and low pass filter $h(\cdot)$ are the detail coefficients (high frequency component coefficients) and the approximation coefficients (low frequency component coefficients), respectively, which are expressed by $D_i(n)$ and $A_i(n)$, respectively. In the process of ChlF signal decomposition, the approximate coefficient A_{i} $_1(n)$ of the j-1th layer is convoluted with $g(\cdot)$ and $h(\cdot)$, respectively, and sampled downward to obtain the detail coefficient D_i and the approximate coefficient A_i of layer j. The ChlF signal x(n) is decomposed according to the number of decomposition levels, as shown in Fig. 1, and the decomposition layers was experimentally determined as 6 in this work. By doing so, a common wavelet entropy index was identified to classify all the samples for different varieties and to illustrate the concept of the proposed work.

The detail coefficients D_j and the approximation coefficients A_j of the $j^{\rm th}$ level of DWT are denoted as:

$$A_j(k) = \sum_{n} x(n)h(2k - n)$$
(3)

$$D_j(k) = \sum_n x(n)g(2k - n) \tag{4}$$

where $g(\cdot)$ is high pass filter; $h(\cdot)$ is low pass filter; $A_j(k)$ is the k^{th} coefficient in the j^{th} approximation of the ChIF signal after wavelet decomposition, which describes the low frequency information of the ChIF signal; $D_j(k)$ is the k^{th} coefficient in the j^{th} detail of the ChIF signal after wavelet decomposition, which describes the high frequency information of the ChIF signal.

2.2. Wavelet entropy

The ChlF signal energy at each scale is expressed as:

$$ED_{j} = \sum_{k} \left| D_{j}(k) \right|^{2} \tag{5}$$

$$EA_{j} = \sum_{k} \left| A_{j}(k) \right|^{2} \tag{6}$$

where j = 1, 2, 3, ..., J, J is the maximum decomposition level, which is 6 in this work

The relative energy for the k^{th} detail at the j^{th} scale is:

$$PD_{j,k} = \frac{D_j(k)}{ED_j} \tag{7}$$

The relative energy for the the k^{th} approximation at the j^{th} scale is:

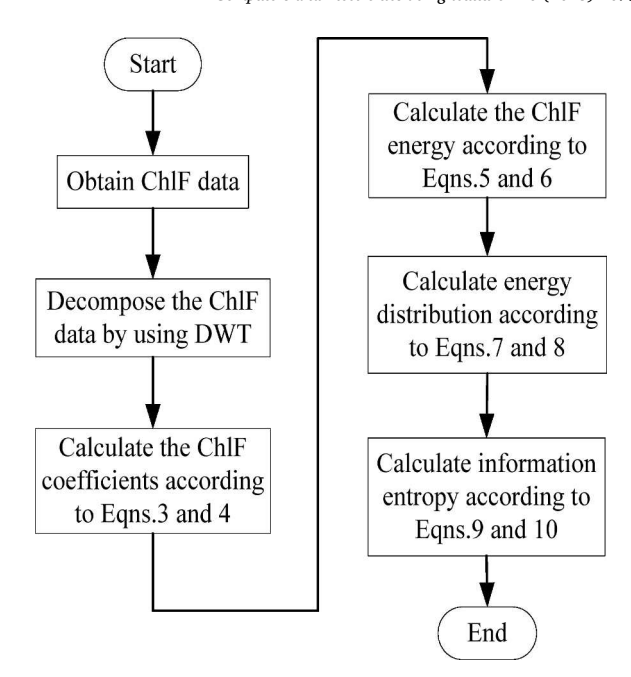


Fig. 2. Flow chart of ChlF wavelet information entropy calculation.

$$PA_{j,k} = \frac{A_j(k)}{EA_j} \tag{8}$$

According to the Shannon information entropy (Ellerman, 2021), the detail information entropy and the approximation information entropy can be calculated. The detail and approximation information entropy of the j^{th} level can be computed as Eqns. (9) and (10), respectively, which will be further used to classify drought stress levels.

$$DE_{j} = -\sum_{k} PD_{j,k}\log(PD_{j,k}) \ PD_{j,k} \in [0, 1]$$
 (9)

$$AE_{j} = -\sum_{k} PA_{j,k} \log(PA_{j,k}) \quad PA_{j,k} \in [0, 1]$$
 (10)

The flow chart of ChlF information entropy calculation is illustrated in Fig. 2.

3. Samples and Experiments

3.1. Plant samples

Rice is one of the most important food crops and spinach is one of the most popular vegetables in the world, thus they are used as samples to test the developed method. Intact and fresh spinach was acquired from a local farmers' market in Wuxi in an early morning in February of 2022. The four rice varieties were Hyou-518 (drought resistant), Zhuliangyou-819 (drought resistant), Xinliangyou-212 (drought susceptible), and Hanyou-2 (drought susceptible). The rice samples were grown in a greenhouse (Wuxi Honeycomb Ecological Agriculture Co., Ltd) in Wuxi city, Jiangsu Province, China.

3.2. Drought stress treatment

Spinach drought stress treatment: The spinach samples were quickly transported to the laboratory for drought stress experiment after purchasing. To reduce the effect of different spinach water status on measured ChIF, the roots of the fresh spinach were put in water for 2 h. Then the spinach samples were kept in an environment with a temperature of 17 $^{\circ}\text{C}$ and air humidity of 40% for 0 h, 3 h, 5 h, and 7 h to induce natural drought stress at different levels. Thirty groups of spinach were

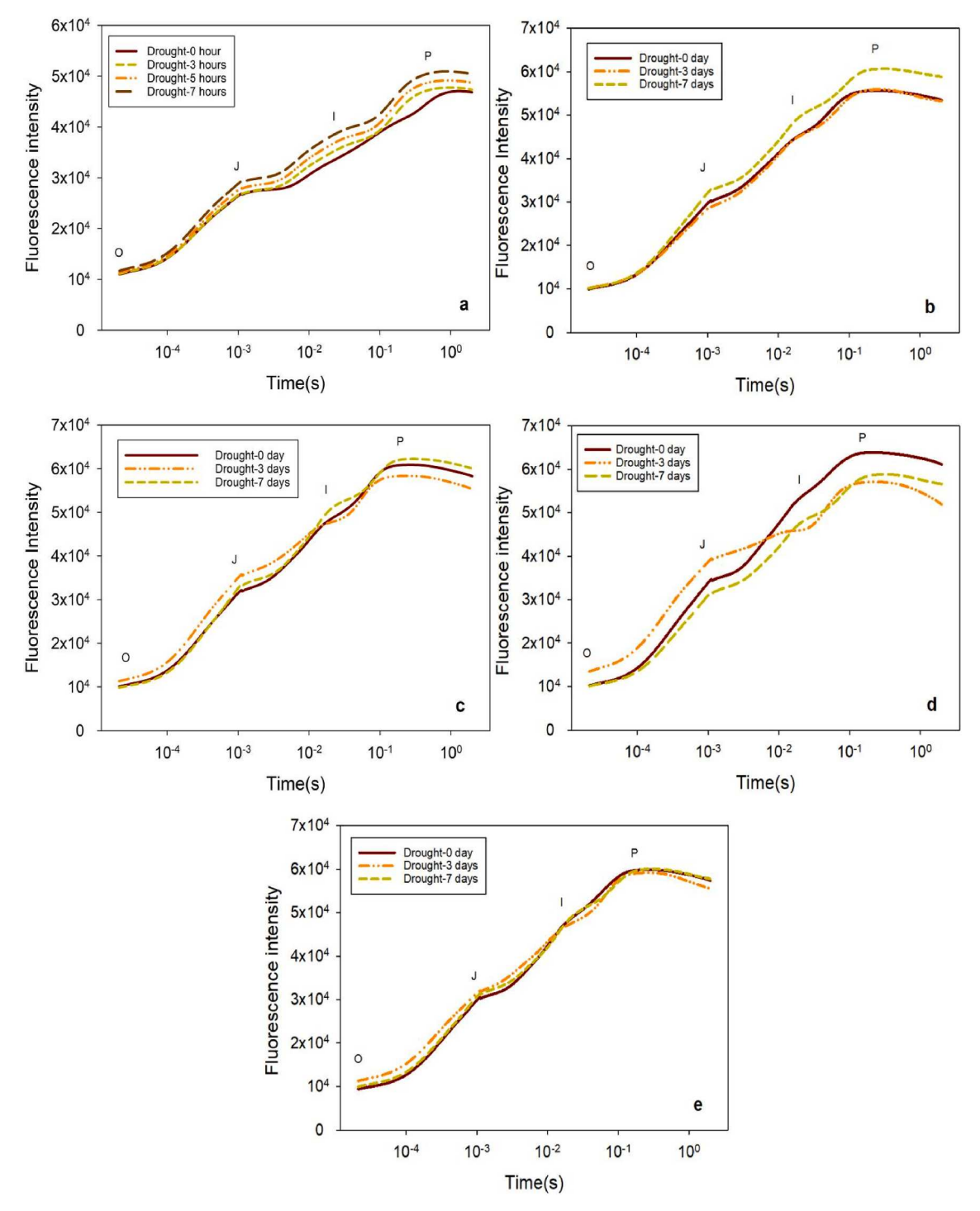


Fig. 3. Illumination light of (a) step light signal, and (b) PRBS light signal.

measured. The spinach samples for the drought experiment were completely exposed in ambient air without water application. This treatment over several hours led to progressive water loss. The spinach weight was measured with an electronic analytical balance (MTB300, Meilen, Guangdong, China) with an accuracy of 0.01 g. The relative water content of the spinach samples was reduced by 3% (fresh weight dry weight)/fresh weight) when the drought treatment lasted for 7 h.

Rice drought stress treatment: Rice seedlings were cultivated in a seedling bed in the greenhouse and kept at 28 $^{\circ}$ C. When the rice seedlings were about 10-cm height, they were transplanted into polyethylene plastic pots (30-cm height and 28-cm in diameter) filled with 10 kg of

paddy soil (soil and chicken manure organic fertilizer in a proportion of 5:1). Six rice seedlings were planted in each pot, and 20 pots of seedings were planted for each variety. The pots were regularly watered before drought stress experiment. At the early stage of rice budding (starting August 24, 2022), the pots were not watered for 0 day, 3 days, and 7 days for inducing natural drought stress. The experiment resulted in 120 sets of ChIF data in total for a rice variety.

3.3. Data acquisition

Leaves were dark-adapted for at least 20 min by using dark-adaption

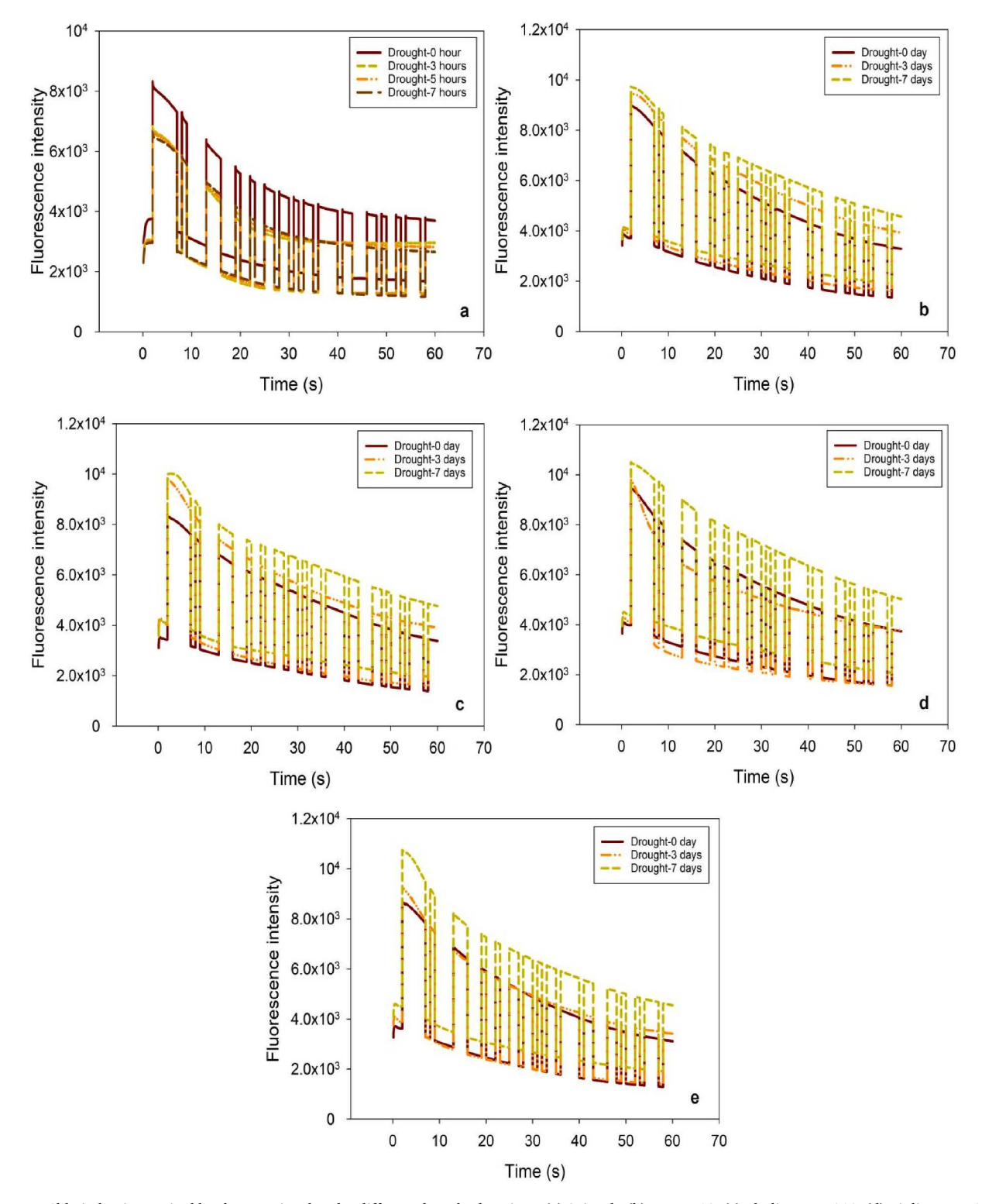


Fig. 4. Mean ChlF induction excited by the step signal under different drought durations. (a) Spinach, (b) Hyou-518, (c) Zhuliangyou-819, (d) Xinliangyou-212, and (e) Hanyou-2.

clips before ChlF measurements. ChlF produced from illumination light with a step signal and a PRBS signal was measured from different leaves (randomly selected for the two types of ChlF measurement) of each plant. The OJIP measurement with a step excitation was performed with a FluorPen PSI (Photon Systems Instruments, Czech Republic) and the PRBS measurement was performed with a FluorX-FX001 ChlF meter (Lushixin Sci. & Tech. Co. Ltd Wuxi, China). Fig. 3 illustrates the step signal and the PRBS signal waveform for exciting ChlF. The step light

intensity was set as 2400 µmol photons $m^{-2}\ s^{-1}$ (Fig. 3a), and the acquisition time was 2 s. The PRBS is generated with seven shift registers (PRBS7) in this work (Refer to, for example, Eriksson et al. (2017) for futher details). The excitation light signal of PRBS is shown in Fig. 3b. The low light intensity and the high light intensity of the PRBS signal was set as 1260 µmol $m^{-2}\ s^{-1}$ and 3150 µmol $m^{-2}\ s^{-1}$ (Fig. 3b), respectively, and the sampling frequency was 100 Hz and the acquisition time was 127 s.

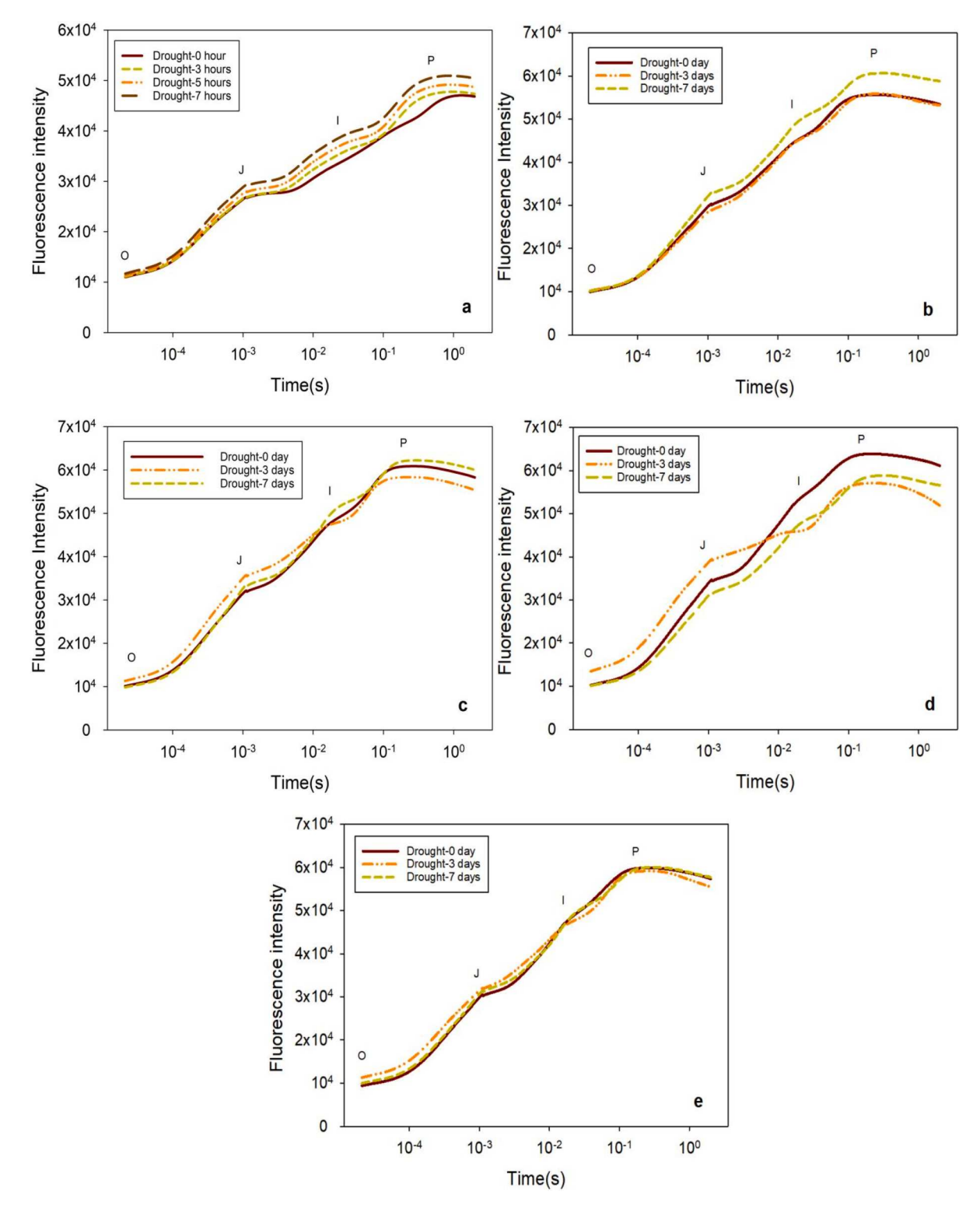


Fig. 5. Mean ChlF induction curves excited by the PRBS signal under different drought durations. (a) Spinach, (b) Hyou-518, (c) Zhuliangyou-819, (d) Xinliangyou-212 and (e) Hanyou-2.

3.4. Data analysis

Discrete wavelet analysis of the PRBS-induced ChlF responses was executed by using Daubechies wavelets in MATLAB (MathWorks, Natick, MA). The number of levels of decomposition was experimentally determined for differentiation of the drought levels. The relative levels of energy in the approximation and each level of details were used to compute the information entropy values.

Statistical analysis was performed in SPSS (Armonk, NY, IBM SPSS Amos 21). The effect of drought stress on the computed ChIF characteristics was assessed by using analysis of variance (ANOVA), least significance difference (LSD), Tamhane-T2, and Kruskal-Wallis nonparametric tests, depending on the normal distribution or homogeneity of variance of the data, at the 5% probability level as done in Yang et al. (2020) and Ma et al. (2022).

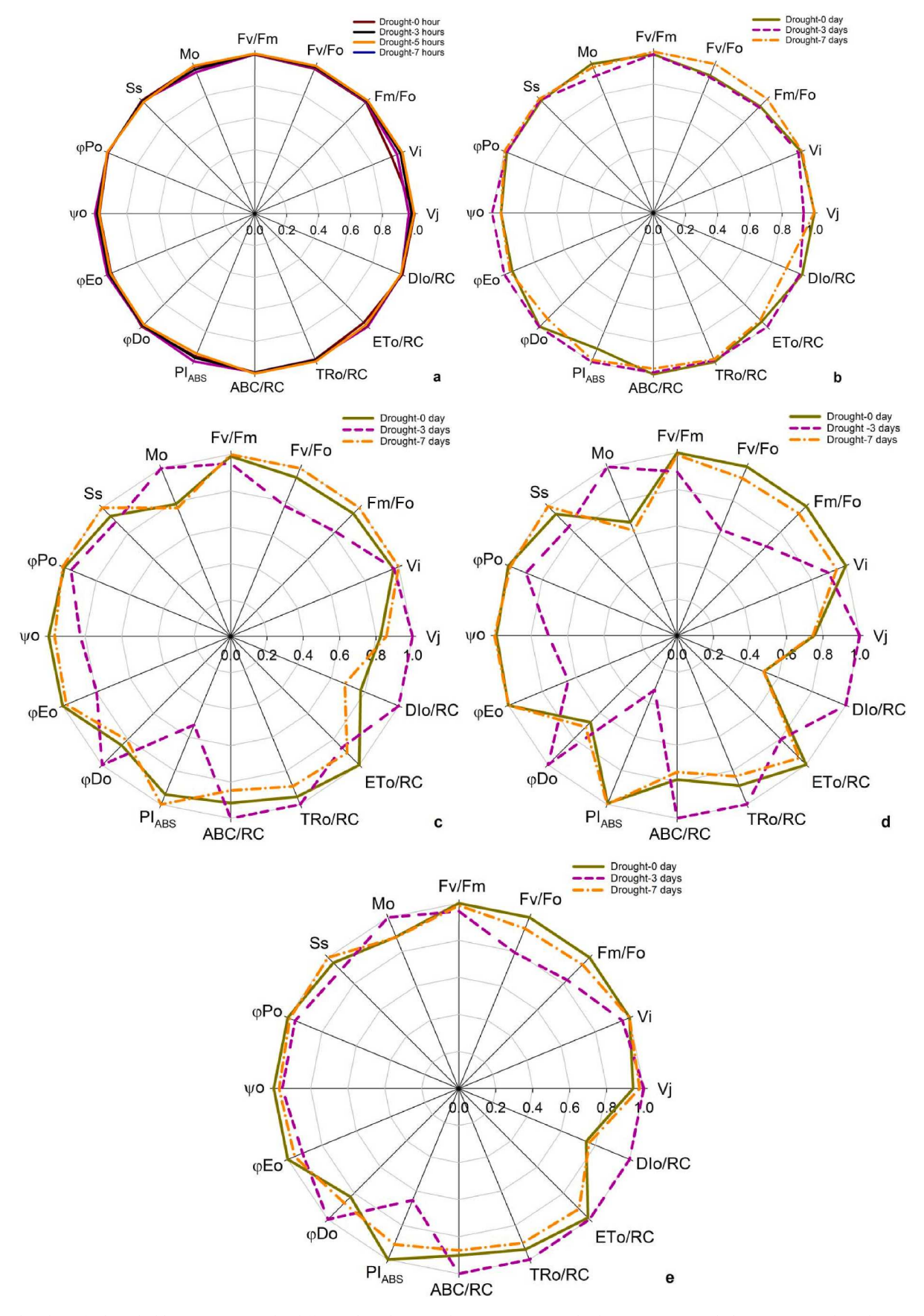


Fig. 6. Spider plots of selected ChlF parameters under different drought stress durations. (a) Spinach, (b) Hyou-518, (c) Zhuliangyou-819, (d) Xinliangyou-212 and (e) Hanyou-2.

Table 1

Statistical analysis of commonly used ChlF features from OJIP induction under different drought stress durations on spinach. Values indicated with different letters in a row are significantly (p < 0.05) different from one another. The results were presented as means \pm standard errors for n = 30. DT1, DT2, DT3, and DT4 refer to non-drought, drought stress for 3 h, drought stress for 5 h, and drought stress for 7 h, respectively.

Parameters	DT1	DT2	DT3	DT4
Vj	$0.45 \pm 0.04a$	$0.43 \pm 0.03 a$	$0.44 \pm 0.03 a$	$0.45\pm0.03a$
Vi	$0.64\pm0.05b$	$0.66\pm0.06ab$	$0.68 \pm 0.06b$	$0.69 \pm 0.06b$
Fm/Fo	$3.99\pm0.52a$	$4.01\pm0.49a$	$4.03\pm0.50a$	$4.05\pm0.48a$
Fv/Fo	$2.99\pm0.52a$	$3.01\pm0.49a$	$3.03\pm0.50a$	$3.05\pm0.48a$
Fv/Fm	$0.74\pm0.04a$	$0.75\pm0.04a$	$0.75\pm0.04a$	$0.75\pm0.04a$
Mo	$0.95 \pm 0.16a$	$0.92\pm0.07a$	$0.93\pm0.06a$	$0.96\pm0.06a$
Ss	$0.48 \pm 0.05a$	$0.47\pm0.04a$	$0.47\pm0.04a$	$0.47\pm0.04a$
φΡο	$0.74\pm0.04a$	$0.75\pm0.04a$	$0.75\pm0.04a$	$0.75\pm0.04a$
ψο	$0.55\pm0.04a$	$0.57\pm0.03a$	$0.56\pm0.03a$	$0.55\pm0.03a$
φΕο	$0.41\pm0.04a$	$0.42\pm0.02a$	$0.42\pm0.02a$	$0.41\pm0.02a$
φDο	$0.26\pm0.04a$	$0.25\pm0.04a$	$0.25\pm0.04a$	$0.25\pm0.04a$
PI_{ABS}	$1.36\pm0.38a$	$1.40\pm0.27a$	$1.37\pm0.27a$	$1.33\pm0.25a$
ABS/RC	$2.87\pm0.46a$	$2.87\pm0.45a$	$2.87\pm0.47a$	$2.89 \pm 0.46a$
TRo/RC	$2.12\pm0.23a$	$2.13\pm0.21a$	$2.13\pm0.21a$	$2.15\pm0.22a$
ETo/RC	$1.17\pm0.14a$	$1.21\pm0.17a$	$1.20\pm0.17a$	$1.19 \pm 0.18 a$
DIo/RC	$0.75\pm0.27a$	$0.74\pm0.26a$	$0.74\pm0.28a$	$0.74\pm0.27a$

4. Results

4.1. ChlF under different drought stress levels

Fig. 4 shows the mean ChlF induction curves excited by the step signal from spinach, Hyou-518, Zhuliangyou-819, Xinliangyou-212, and Hanyou-2 under different drought stress durations. Fig. 5 shows the mean ChlF induction curves excited by the PRBS signal from spinach, Hyou-518, Zhuliangyou-819, Xinliangyou-212, and Hanyou-2 under

different drought stress durations (Fig. 5 shows only the ChIF data of the first 60 s). It can be seen that there is not a consistent observable difference in the ChIF induction curves between non-drought and drought-stressed samples from Figs. 4 and 5.

4.2. Effects of drought stress on traditional ChlF features

In order to show the difference in the ChIF parameters of the OJIP induction of spinach and rice under different drought stress durations, the ChIF values were normalized by the maximum value in each group. The normalized ChIF parameters of ChIF are shown in spider plots. The ChIF parameter values of spinach under different drought stress levels are almost the same in Fig. 6a (p>0.05). The ChIF parameters of Zhuliangyou-819 and Xinliangyou-212 with drought stress for 3 days are different from those with non-drought and drought stress for 7 days (p<0.05, Fig. 6c and 6d). The ChIF parameter values of rice in non-drought and drought stress for 7 days are very close (p>0.05, Fig. 6 (b-e)).

Statistical comparisons of ChIF parameters of spinach and the four rice varieties among different drought stress durations are presented in Tables 1 and 2. ChIF parameters Vi shows statistical differences (p < 0.05) between non-drought and drought stress exceeding 5 h, and most of the traditional ChIF features from OJIP induction of spinach have no statistical difference between different drought stress durations (Table 1).

Effects of different drought durations on rice on the ChlF parameters are shown in Table 2. It can be observed that the ChlF parameters (Fm/Fo, Fv/Fo, Fv/Fm, Ss, ϕ Po, ϕ Do, PI_{ABS}, ABS/RC, and TRo/RC) of Zhuliangyou-819, Xinliangyou-212, and Hanyou-2 are statistically different between drought stress levels, but Hyou-518 under different drought stress durations cannot be distinguished (p > 0.05). Although ChlF parameter ϕ Eo of Zhuliangyou-819 and Hanyou-2 are statistically

Table 2 Statistical analysis of commonly used ChIF features from OJIP induction under different drought stress durations on rice. Values indicated with different letters in a row are significantly (p < 0.05) different. The results were presented as means \pm standard errors for n = 120. I, II, III, and IV represent Hyou-518, Zhuliangyou-819, Xinliangyou-212, and Hanyou-2. Dd1, Dd2, and Dd3 refer to non-drought, drought stress for 3 days, and drought stress for 7 days, respectively.

Varieties & parameters	Dd1	Dd2	Dd3	Varieties & parameters	Dd1	Dd2	Dd3
I-Vj	$0.47 \pm 0.04a$	$0.44\pm0.03b$	$0.47 \pm 0.03a$	Ι-ψο	$0.53 \pm 0.04b$	$0.56 \pm 0.03a$	$0.53 \pm 0.03b$
II-Vj	$0.45\pm0.02c$	$0.54\pm0.08a$	$0.47\pm0.02b$	ΙΙ-ψο	$0.55\pm0.02a$	$0.46\pm0.08c$	$0.53\pm0.02b$
III-Vj	$0.47\pm0.02b$	$0.62\pm0.12a$	$0.46\pm0.04b$	ΙΙΙ-ψο	$0.53\pm0.02a$	$0.38 \pm 0.12 b$	$0.54 \pm 0.04a$
IV-Vj	$0.43\pm0.02b$	$0.46\pm0.04a$	$0.45\pm0.04~\text{s}$	ΙV-ψο	$0.57\pm0.02a$	$0.54\pm0.04b$	$0.55\pm0.04b$
I-Vi	$0.81\pm0.02a$	$0.79\pm0.03b$	$0.81\pm0.02a$	Ι-φΕο	$0.43\pm0.04b$	$0.45\pm0.03a$	$0.44\pm0.02b$
II-Vi	$0.78\pm0.02a$	$0.79\pm0.03c$	$0.81\pm0.02b$	ΙΙ-φΕο	$0.45\pm0.02a$	$0.36\pm0.07c$	$0.44\pm0.02b$
III-Vi	$0.84 \pm 0.02a$	$0.76\pm0.08c$	$0.80\pm0.02b$	ΙΙΙ-φΕο	$0.44\pm0.03a$	$0.28\pm0.10b$	$0.44\pm0.04a$
IV-Vi	$0.81\pm0.02a$	$0.78\pm0.02b$	$0.81\pm0.02a$	ΙV-φΕο	$0.47\pm0.02a$	$0.43\pm0.04c$	$0.45\pm0.03b$
I-Fm/Fo	$5.22\pm0.48a$	$5.17\pm0.27a$	$5.57\pm0.33a$	Ι-φDο	$0.19\pm0.02a$	$0.19\pm0.01a$	$0.18\pm0.01b$
II-Fm/Fo	$5.61\pm0.35b$	$4.79\pm0.53c$	$5.87 \pm 0.28a$	ΙΙ-φDο	$0.18\pm0.01b$	$0.21\pm0.02a$	$0.17\pm0.01c$
III-Fm/Fo	$5.75 \pm 0.45a$	$3.98\pm0.72c$	$5.43\pm0.29b$	III-φDo	$0.18\pm0.01b$	$0.26\pm0.05a$	$0.18\pm0.01c$
IV-Fm/Fo	$5.91\pm0.30a$	$4.90\pm0.28c$	$5.59\pm0.26b$	IV-φDo	$0.17\pm0.01c$	$0.20\pm0.01a$	$0.18\pm0.01b$
I-Fv/Fo	$4.22\pm0.48b$	$4.17\pm0.27b$	$4.57\pm0.33a$	I-PI _{ABS}	$2.20\pm0.69b$	$2.41\pm0.47a$	$2.38\pm0.39a$
II-Fv/Fo	$4.61\pm0.35b$	$3.79\pm0.53c$	$4.87\pm0.28a$	II-PI _{ABS}	$2.49\pm0.45b$	$1.39\pm0.64c$	$2.65\pm0.44a$
III-Fv/Fo	$4.75\pm0.45a$	$2.98\pm0.72c$	$4.43\pm0.29b$	III-PI _{ABS}	$2.39 \pm 0.58a$	$0.78\pm0.56b$	$2.41\pm0.55a$
IV-Fv/Fo	$4.91\pm0.30a$	$3.90\pm0.28b$	$4.59\pm0.26c$	IV-PI _{ABS}	$2.97\pm0.48a$	$1.94\pm0.46c$	$2.70\pm0.55b$
I-Fv/Fm	$0.81\pm0.02ab$	$0.81\pm0.01b$	$0.82\pm0.01a$	I-ABS/RC	$2.29\pm0.19a$	$2.26\pm0.11a$	$2.21\pm0.13b$
II-Fv/Fm	$0.82\pm0.01b$	$0.79\pm0.02c$	$0.83\pm0.01a$	II-ABS/RC	$2.32\pm0.16b$	$2.53\pm0.19a$	$2.14\pm0.14c$
III-Fv/Fm	$0.83\pm0.01a$	$0.74\pm0.05c$	$0.82\pm0.01b$	III-ABS/RC	$2.34\pm0.20b$	$2.97\pm0.57a$	$2.22\pm0.14c$
IV-Fv/Fm	$0.83 \pm 0.01 a$	$0.80\pm0.01c$	$0.82\pm0.01b$	IV-ABS/RC	$2.22\pm0.14b$	$2.47\pm0.14a$	$2.16\pm0.13c$
I-Mo	$0.87\pm0.12a$	$0.80\pm0.08b$	$0.85\pm0.07a$	I-TRo/RC	$1.84\pm0.11a$	$1.82\pm0.07ab$	$1.81\pm0.09b$
II-Mo	$0.85\pm0.08b$	$1.09 \pm 0.18 a$	$0.83\pm0.08b$	II-TRo/RC	$1.90\pm0.11b$	$1.99 \pm 0.11a$	$1.78\pm0.10c$
III-Mo	$0.90\pm0.10b$	$1.34\pm0.29a$	$0.83\pm0.11c$	III-TRo/RC	$1.93\pm0.14b$	$2.17\pm0.25a$	$1.81\pm0.10c$
IV-Mo	$0.80\pm0.07b$	$0.90\pm0.11a$	$0.79\pm0.10b$	IV-TRo/RC	$1.84\pm0.10b$	$1.96\pm0.10a$	$1.77\pm0.10c$
I-Ss	$0.54\pm0.03a$	$0.55\pm0.02a$	$0.55\pm0.03a$	I-ETo/RC	$0.97\pm0.04b$	$1.02\pm0.04a$	$0.96 \pm 0.06b$
II-Ss	$0.53\pm0.03b$	$0.50\pm0.03c$	$0.57\pm0.03a$	II-ETo/RC	$1.04\pm0.05a$	$0.90\pm0.16c$	$0.95 \pm 0.05b$
III-Ss	$0.52\pm0.04b$	$0.47\pm0.04c$	$0.56\pm0.03a$	III-ETo/RC	$1.02\pm0.05a$	$0.82\pm0.30c$	$0.97\pm0.07b$
IV-Ss	$0.54\pm0.03b$	$0.51\pm0.03c$	$0.57\pm0.03a$	IV-ETo/RC	$1.05\pm0.05a$	$1.06\pm0.07a$	$0.98\pm0.05b$
Ι-φΡο	$0.81\pm0.02b$	$0.81\pm0.01b$	$0.82\pm0.01a$	I-DIo/RC	$0.45\pm0.08a$	$0.44\pm0.04a$	$0.40\pm0.05b$
ΙΙ-φΡο	$0.82\pm0.01b$	$0.79\pm0.02c$	$0.83\pm0.01a$	II-DIo/RC	$0.42\pm0.06b$	$0.54 \pm 0.10a$	$0.37\pm0.04c$
III-φPo	$0.83\pm0.01a$	$0.74\pm0.05c$	$0.82\pm0.01b$	III-DIo/RC	$0.41\pm0.07b$	$0.80\pm0.34a$	$0.41\pm0.04b$
ΙV-φΡο	$0.83\pm0.01a$	$0.8\pm0.010c$	$0.82\pm0.01b$	IV-DIo/RC	$0.38\pm0.04b$	$0.51\pm0.06a$	$0.39\pm0.04b$

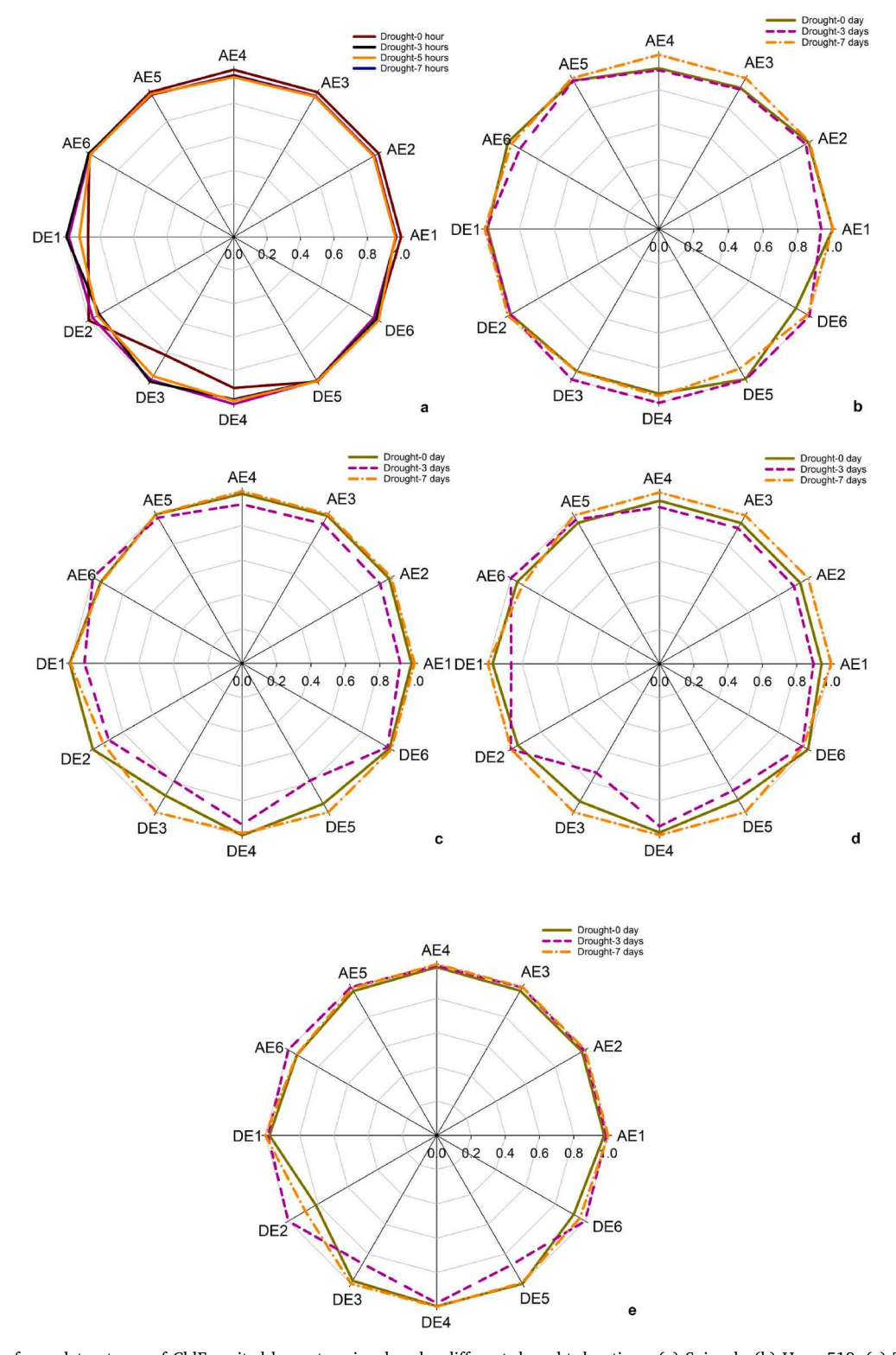


Fig. 7. Spider plots of wavelet entropy of ChlF excited by a step signal under different drought durations. (a) Spinach, (b) Hyou-518, (c) Zhuliangyou-819, (d) Xinliangyou-212, and (e) Hanyou-2. (AEi and DEi represent the wavelet entropy of the ith (i = 1, 2, ... 6) approximation and detail components, respectively.).

different under different drought stress durations, these parameters cannot distinguish Hyou-518 and Zhuliangyou-819 under different drought stress durations, and this is also for ChlF parameter ETo/RC. All the commonly-used ChlF parameters cannot fully distinguish Hyou-518 under different drought durations.

In sum, from the results of Tables 1 and 2, there is no one parameter from the OJIP ChlF induction that can completely distinguish either

spinach or rice under different drought duartions and genetic varieties.

4.3. Effects of drought stress on wavelet entropy of ChlF excited by a step signal

Fig. 7 shows spider plots of wavelet entropy of ChlF from the spinach and the four rice varieties excited by a step signal under different

Table 3 Statistical analysis of wavelet entropy of spinach ChlF under different drought durations excited by a step signal. Values indicated with different letters in a column are significantly (p < 0.05) different. The results of ChlF were presented as means \pm standard errors for n = 30. DT1, DT2, DT3, and DT4 refer to non-drought, drought stress for 3 h, drought stress for 5 h, and drought stress for 7 h, respectively. AEi and DEi represent the wavelet entropy of the ith (i = 1, 2, ... 6) approximation and detail component, respectively.

Scale and	l Stress level	Entropy	Scale and	Stress	Entropy	Scale and	Stress level	Entropy
AE1	DT1	$2.77 \pm 0.07a$	AE2	DT1	$2.81 \pm 0.05a$	AE3	DT1	$2.83 \pm 0.05a$
	DT2	$2.69\pm0.04b$		DT2	$2.73\pm0.04b$		DT2	$2.76\pm0.04b$
	DT3	$2.68\pm0.04b$		DT3	$2.72\pm0.04\mathrm{b}$		DT3	$2.75\pm0.03b$
	DT4	$2.67\pm0.05b$		DT4	$2.71\pm0.05\mathrm{b}$		DT4	$2.75\pm0.04b$
AE4	DT1	$2.79\pm0.04a$	AE5	DT1	$2.52 \pm 0.08a$	AE6	DT1	$2.37\pm0.07a$
	DT2	$2.70\pm0.06b$		DT2	$2.48\pm0.07b$		DT2	$2.36\pm0.10a$
	DT3	$2.68\pm0.05b$		DT3	$2.48\pm0.08b$		DT3	$2.37\pm0.08a$
	DT4	$2.66\pm0.05b$		DT4	2.49 ± 0.06 ab		DT4	$2.34\pm0.09a$
DE1	DT1	$0.21\pm0.15a$	DE2	DT1	$1.15\pm0.29a$	DE3	DT1	$1.03\pm0.14b$
	DT2	$0.24\pm0.22a$		DT2	$1.11\pm0.27a$		DT2	$1.25\pm0.18a$
	DT3	$0.24\pm0.24a$		DT3	$1.06\pm0.31a$		DT3	$1.26\pm0.21a$
	DT4	$0.23\pm0.20a$		DT4	$1.08 \pm 0.28 a$		DT4	$1.22\pm0.18a$
DE4	DT1	$1.62\pm0.14b$	DE5	DT1	$2.12\pm0.18a$	DE6	DT1	$2.30\pm0.24a$
	DT2	$1.80\pm0.15a$		DT2	$2.11\pm0.14a$		DT2	$2.25\pm0.17a$
	DT3	$1.75\pm0.15a$		DT3	$2.11\pm0.17a$		DT3	$2.29\pm0.13a$
	DT4	$1.76\pm0.15a$		DT4	$2.12\pm0.14a$		DT4	$2.33\pm0.14a$

Table 4
Statistical analysis of wavelet entropy of rice ChlF under different drought durations excited by a step signal. Values indicated with different letters in a row are significantly (p < 0.05) different from one another. The results about ChlF were presented as means \pm standard errors values for n = 120. I, II, III, and IV represent Hyou-518, Zhuliangyou-819, Xinliangyou-212, and Hanyou-2. Dd1, Dd2, and Dd3 refer to non-drought, drought stress for 3 days, and stress drought for 7 days, respectively. AEi and DEi represent the wavelet entropy of the ith (i = 1, 2, ... 6) approximation and detail components, respectively.

Varieties & Scales	Dd1	Dd2	Dd3	Varieties & Scales	Dd1	Dd2	Dd3
I-AE1	$2.51\pm0.06b$	$2.60 \pm 0.05 a$	$2.61\pm0.06a$	I-AE2	$2.55\pm0.06b$	$2.64 \pm 0.05a$	$2.65\pm0.05a$
I-AE3	$2.57\pm0.06b$	$2.66\pm0.05a$	$2.67\pm0.05a$	I-AE4	$2.54\pm0.08b$	$2.63\pm0.06a$	$2.65\pm0.06a$
I-AE5	$2.31\pm0.11b$	$2.40\pm0.05a$	$2.40\pm0.05a$	I-AE6	$1.99\pm0.14a$	$1.92\pm0.11b$	$1.98\pm0.14b$
I-DE1	$0.18\pm0.01b$	$0.18 \pm 0.01a$	$0.18 \pm 0.00 ab$	I-DE2	$1.00\pm0.27a$	$0.98 \pm 0.25a$	$0.92\pm0.23a$
I-DE3	$1.06\pm0.23a$	$1.07\pm0.14a$	$1.21\pm0.17a$	I-DE4	$1.58\pm0.13b$	$1.63\pm0.13a$	$1.64\pm0.09a$
I-DE5	$1.98\pm0.18b$	$1.99 \pm 0.24b$	$2.16\pm0.14a$	I-DE6	$2.05\pm0.24ab$	$2.25\pm0.20a$	$1.98\pm0.29b$
II-AE1	$2.59\pm0.06b$	$2.42\pm0.13c$	$2.63\pm0.06a$	II-AE2	$2.63\pm0.05b$	$2.47\pm0.12c$	$2.67\pm0.05a$
II-AE3	$2.65\pm0.05b$	$2.51\pm0.12c$	$2.68\pm0.05a$	II-AE4	$2.63\pm0.06b$	$2.47\pm0.12c$	$2.67\pm0.06a$
II-AE5	$2.40\pm0.06b$	$2.35 \pm 0.10b$	$2.40\pm0.04a$	II-AE6	$1.99 \pm 0.14a$	$2.11\pm0.10a$	$1.98\pm0.14b$
II-DE1	$0.18 \pm 0.01a$	$0.17\pm0.02b$	$0.18\pm0.00b$	II-DE2	$0.96\pm0.24a$	$0.85 \pm 0.23c$	$0.89 \pm 0.20b$
II-DE3	$1.09 \pm 0.16b$	$0.97\pm0.18c$	$1.23\pm0.16a$	II-DE4	$1.65\pm0.10a$	$1.55\pm0.11b$	$1.63\pm0.06a$
II-DE5	$2.02\pm0.24b$	$1.69 \pm 0.23c$	$2.15\pm0.13a$	II-DE6	$2.11\pm0.23a$	$2.08\pm0.25a$	$2.14\pm0.33a$
III-AE1	$2.48\pm0.06b$	$2.35\pm0.20c$	$2.62\pm0.07a$	III-AE2	$2.52\pm0.06b$	$2.41\pm0.20c$	$2.66\pm0.06a$
III-AE3	$2.55\pm0.05b$	$2.45\pm0.20c$	$2.68\pm0.06a$	III-AE4	$2.52\pm0.07b$	$2.43\pm0.20c$	$2.65\pm0.07a$
III-AE5	$2.27\pm0.08c$	$2.33 \pm 0.21b$	$2.39\pm0.05a$	III-AE6	$2.06\pm0.13b$	$2.16\pm0.14a$	$1.99\pm0.14c$
III-DE1	$0.18 \pm 0.01b$	$0.16\pm0.03c$	$0.18\pm0.01a$	III-DE2	$0.90\pm0.20a$	$0.94 \pm 0.29a$	$0.94\pm0.23a$
III-DE3	$1.10 \pm 0.16 b$	$0.87 \pm 0.17c$	$1.19 \pm 0.17a$	III-DE4	$1.61\pm0.12a$	$1.55\pm0.17b$	$1.64\pm0.08a$
III-DE5	$1.93\pm0.24b$	$1.80\pm0.26c$	$2.10\pm0.17a$	III-DE6	$2.21\pm0.24a$	$2.13\pm0.28b$	$2.14\pm0.26b$
IV-AE1	$2.56\pm0.05c$	$2.59 \pm 0.07 b$	$2.62\pm0.06a$	IV-AE2	$2.60\pm0.06b$	$2.64\pm0.07a$	$2.65\pm0.06a$
IV-AE3	$2.61\pm0.06b$	$2.67 \pm 0.07a$	$2.68\pm0.05a$	IV-AE4	$2.60\pm0.06c$	$2.63\pm0.08b$	$2.65\pm0.06a$
IV-AE5	$2.36\pm0.09b$	$2.42\pm0.07a$	$\textbf{2.40} \pm \textbf{0.05a}$	IV-AE6	$1.93\pm0.12b$	$2.06\pm0.15a$	$1.94\pm0.12b$
IV-DE1	$0.18 \pm 0.01b$	$0.18 \pm 0.01 \text{ab}$	$0.19\pm0.01a$	IV-DE2	$0.85\pm0.16b$	$1.05\pm0.29a$	$0.93\pm0.24b$
IV-DE3	$1.21\pm0.21a$	$1.07\pm0.21b$	$1.24\pm0.19a$	IV-DE4	$1.66\pm0.10a$	$1.63\pm0.15b$	$1.67\pm0.09a$
IV-DE5	$2.18\pm0.18 a$	$1.90\pm0.29b$	$2.17\pm0.15a$	IV-DE6	$2.06\pm0.23b$	$2.24\pm0.22a$	$2.16\pm0.29a$

drought stress durations. The difference of normalized wavelet entropy values of Zhuliangyou-819 (wavelet entropy DE2, DE3, and DE5), Xinliangyou-212 (wavelet entropy AE1, AE2, AE3, AE4, DE3, and DE5), and Hanyou-2 (wavelet entropy DE2) among different drought durations can be seen from Fig. 7c-7e, but there is not a single feature that can differentiate all the samples under different drought stress durations.

The ChIF of spinach and four rice varieties under different drought durations excited by a step signal was subjected to wavelet decomposition, and the entropy values of the detail component and the approximate component of each level of decomposition and their statistical comparisons among different drought durations are shown in Tables 4 and 5, respectively. Although the wavelet entropy of the approximate components (AE1, AE2, AE3, and AE4) and detail components (DE3 and DE4) of spinach are statistically different between non-drought and drought-stressed samples, there is no statistical differences among

drought-stressed samples. (Table 3).

Different drought durations have significant effects on the wavelet entropy of approximate components (AE1 and AE4) of Zhuliangyou-819, Xinliangyou-212, and Hanyou-2 as shown in Table 4. In addition, although the wavelet entropy of approximate components (AE2 and AE3) and detail components (DE3 and DE5) of Zhuliangyou-819 and Xinliangyou-212 show significant statistical differences among different drought durations, the wavelet entropy cannot completely distinguish Hyou-518 or Hanyou-2 under different drought durations. The wavelet entropy of approximate components (AE1, AE2, AE3, AE4, AE5, AE6, and DE4) for Hyou-518 are statistically different between non-drought and drought stress treated samples, but there is no statistical difference in these parameters between samples with drought stressed for 3 days and 7 days. In sum, none of the wavelet entropy values in Tabels 3 and 4 can completely distinguish spinach and rice under different drought durations.

Table 5 Statistical analysis of wavelet entropy of spinach ChlF under different drought durations excited the PRBS signal. Values indicated with different letters in a column are significantly (p < 0.05) different from one another. The results are presented as means \pm standard errors for n = 30. DT1, DT2, DT3, and DT4 refer to non-drought, drought stress for 3 h, drought stress for 5 h and drought stress for 7 h, respectively. AEi and DEi represent the wavelet entropy of the ith (i = 1, 2, ... 6) approximation and detail components, respectively.

Scale and	d Stress level	Entropy	Scale and	l Stress	Entropy	Scale and	Stress level	Entropy
AE1	DT1	$3.23 \pm 0.24 \text{a}$	AE2	DT1	$3.12\pm0.25a$	AE3	DT1	$3.27\pm0.23a$
	DT2	$2.58\pm0.25d$		DT2	$\textbf{2.45} \pm \textbf{0.23d}$		DT2	$2.72\pm0.23c$
	DT3	$2.86\pm0.26c$		DT3	$2.73\pm0.22c$		DT3	$2.92\pm0.23b$
	DT4	$3.03\pm0.24b$		DT4	$2.94\pm0.22b$		DT4	$3.07\pm0.22b$
AE4	DT1	$3.36\pm0.21a$	AE5	DT1	$3.44 \pm 0.19a$	AE6	DT1	$3.51\pm0.19b$
	DT2	$2.87\pm0.20c$		DT2	$3.05\pm0.17c$		DT2	$3.26\pm0.17c$
	DT3	$3.06\pm0.21b$		DT3	$3.18\pm0.18b$		DT3	$3.32\pm0.16bc$
	DT4	$3.19 \pm 0.22b$		DT4	$3.28\pm0.20b$		DT4	$3.37\pm0.17a$
DE1	DT1	$0.29 \pm 0.11 ab$	DE2	DT1	$0.79\pm0.24b$	DE3	DT1	$0.91\pm0.21a$
	DT2	0.33 ± 0.10 a		DT2	$1.02 \pm 0.16 a$		DT2	$0.96 \pm 0.23a$
	DT3	$0.27 \pm 0.05b$		DT3	$0.77\pm0.18b$		DT3	$0.84 \pm 0.11a$
	DT4	$0.27\pm0.06b$		DT4	$0.77\pm0.17b$		DT4	$0.88 \pm 0.21a$
DE4	DT1	$1.59 \pm 0.17 ab$	DE5	DT1	$2.60\pm0.13b$	DE6	DT1	$3.26\pm0.12ab$
	DT2	$1.66 \pm 0.17a$		DT2	$2.70\pm0.11a$		DT2	$3.27\pm0.10a$
	DT3	$1.56\pm0.10b$		DT3	$2.61\pm0.06b$		DT3	$3.24\pm0.10ab$
	DT4	$1.62 \pm 0.17 \text{ab}$		DT4	$2.56\pm0.06b$		DT4	$3.21\pm0.10b$

4.4. Effects of drought stress on the wavelet entropy of ChlF excited by the PRBS signal

The normalized wavelet entropy values of ChlF excited by the PRBS signal under different drought stress durations are shown in Fig. 8. Most of wavelet entropy values show differences among different drought stress durations as detailed next. In particular, wavelet approximate components AE1, AE2, AE3, AE4, and AE5 of spinach in Fig. 8a show differences while they do not in Fig. 6a and Fig. 7a.

Tables 5 and 6 compare the wavelet entropy values of ChlF of spinach and the four different rice genetic varieties excited by the PRBS signal. There are statistically significance differences in the wavelet entropy of the approximation components (AE1 and AE2) among spinach drought levels (Table 5). The wavelet entropy of the approximation components (AE1, AE2, AE3, AE4, and AE5) of the four rice varieties all show statistically significant differences among drought levels (Table 6).

It can be seen from the results in Tables 5 and 6 that the wavelet entropy of the approximation components AE1 and AE2 of ChlF excited by the PRBS signal show significant differences among all drought stress levels, and can distinguish spinach and four varieties of rice under different drought levels. Therefore, the wavelet entropy of the approximation components AE1 and AE2 parameter of the PRBS-based ChlF signal may serve as a measure to differentiate drought stress levels in spinach and the rice varieties.

5. Discussion

Drought stress reduces water content, increases stomatal resistance, reduces transpiration, affects the synthesis of plant chlorophyll, accelerates the decomposition of chlorophyll, reduces chlorophyll content, and finally reduces the photosynthetic rate of crops (Wu et al., 2008; Li et al., 2021). ChlF from PSII does not only reflect the efficiency of photochemistry, but also reflect the structure of PSII photosynthesis (Lazár, 2006). The relative ChlF values under drought stress were higher than non-drought group for the J-step and I-step (Wang et al., 2018). In our study, the ChlF values of spinach at J, I, and P steps under drought were higher than those without drought, and the fluorescence value increased with the longer drought durations (Fig. 1, Table 1). The ChlF values of Zhuliangyou-819 and Hanyou-2 at the J-step under drought were higher than those without drought, but this was not observed in Hyou-518 and Xinliangyou-212 (Fig. 1, Table 1).

ChlF parameters from the common OJIP induction curve have been widely used to determine photosynthetic traits in the literature

(Tribulato et al., 2019; Mathobo et a., 2017; Stirbet et al., 2018), including the effect of drought stress on crops (Faseela et al., 2019). It is reported that Fv/Fm decreases significantly under drought stress conditions (Xiao et al., 2019; Xu et al., 2020). In our results, the ChIF parameters (Fm/Fo, Fv/Fo, Fv/Fm, and φPo) of spinach under drought stress were larger than those under non-drought condition, Ss and φDo under non-drought condition were larger than those under drought condition (Table 1). However, the ChlF parameters (Fm/Fo, Fv/Fo, Fv/ Fm, and φPo) of Xinliangyou-212 and Hanyou-2 under non-drought condition were larger than those under drought stress. In addition, Ss of Hyou-518 and ϕ Do of Hanyou-2 under drought conditions were larger than that under non-drought stress condition (Table 2). This result is inconsistent with the result in Table 1. φEo of Zhuliangyou-819 and Hanyou-2 decreased under drought stress, which is consistent with the research of Wang et al. (2018), but is inconsistent for Hyou-518 (Table 2). DIo/RC of Hanyou-2 with drought stress was larger than that without drought stress, but this parameter of Hyou-518 with drought was less than that with non-drought stress (Table 2). Therefore, there are differences in the changes of the same OJIP-based ChlF parameters among different plants or varieties under drought stress. Statistical analysis of OJIP-based ChlF parameters shows that there is not one OJIP-based ChlF parameter capable of distinguishing different drought conditions for spinach and the four rice varieties (Tables 2 and

Since drought stress affects electron transport in plants, it will affect ChlF signal dynamics in the time domain or the frequency domain, but the effects may not be observable from a narrow-band-excited ChlF signal. A broad-band excitation signal may stimulate the system to produce ChlF with rich dynamics in the time domain or more frequency components in the frequency domain to reflect the ChlF dynamics affected by drought stress. This work thus focused on whether the wavelet information entropy of ChlF excited by the broad-band PRBS signal could reflect the impact of drought stress on plants, and the results were compared with the results from the traditional OJIP induction. Compared with step excitation, PRBS excitation resulted in more wavelet information entropy values that could differentiate more drought stress levels for spinach and rice varieties as shown in Tables 5 and 6. The results validate the idea that a broadband signal would perturb more dynamic characteristics of the photosynthetic system to carry more information on drought stress, which can be perceived by the wavelet information entropy. The wavelet information entropy of the 1st-level and the 2nd-level approximation component ChlF excited by the PRBS signal was able to differentiate all drought stress levels for all rice varieties and spinach. The low-frequency components of the ChlF

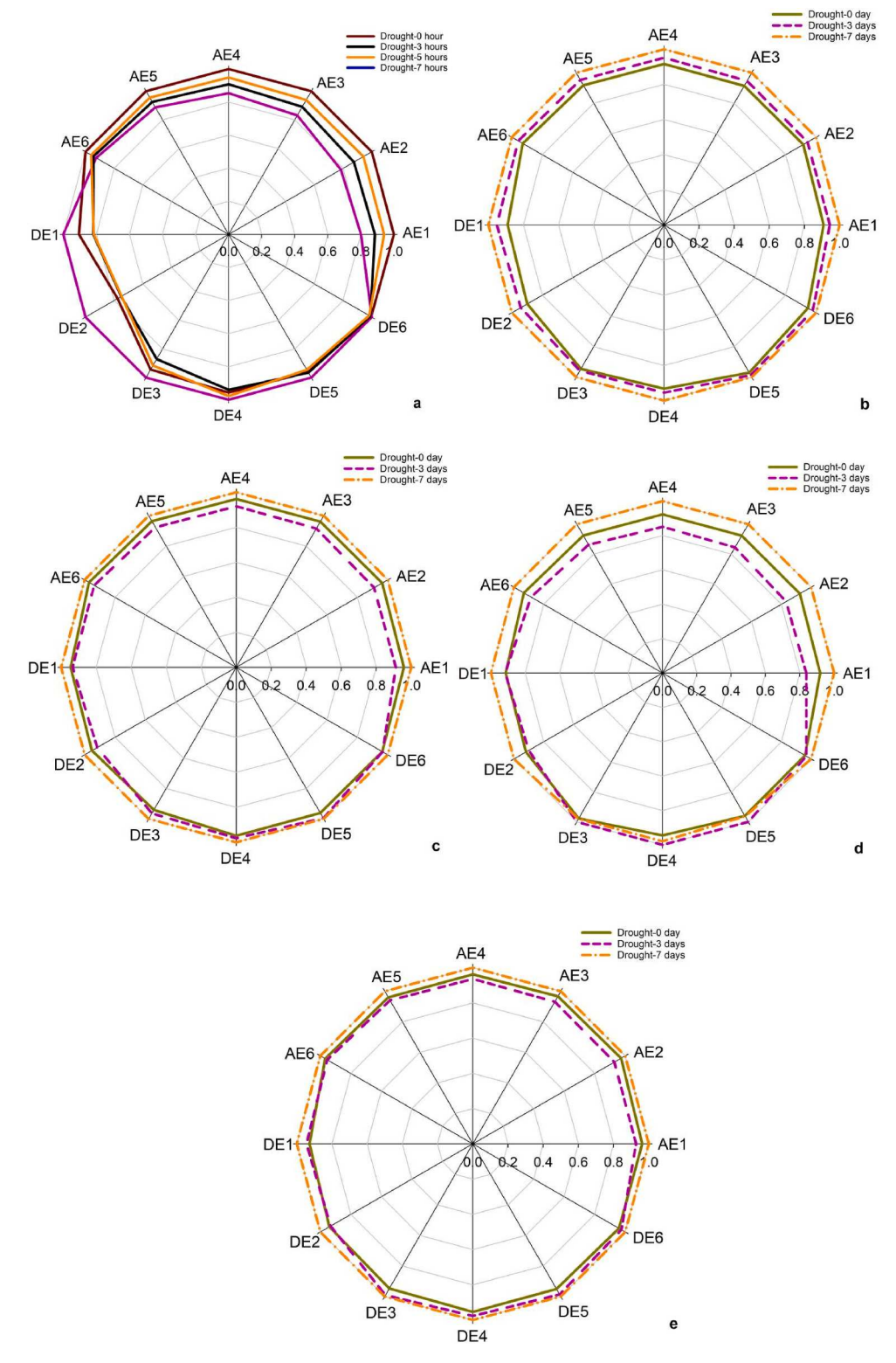


Fig. 8. Spider plots of wavelet entropy of ChlF excited by the PRBS signal under different drought stress durations. (a) Spinach, (b) Hyou-518, (c) Zhuliangyou-819, (d) Xinliangyou-212, and (e) Hanyou-2. (AEi and DEi represent the wavelet entropy of the ith (i = 1, 2, ... 6) approximation and detail components, respectively.).

signal is greatly affected by drought stress. This provides evidence for further research and development of ChlF sensing technique with PRBS excitation. The measurement time of the PRBS-based ChlF is longer than the OJIP induction measurement, which seems to be a disadvantage of the developed method at this stage of the research. Robust identification of drought stress, however, is more important than fast measurement and dark-adaptation takes much longer time than the ChlF signal

measurement itself does in both scenarios. Thus, the relative longer measurement time of PRBS-based ChlF should not be a major reason impeding its field applications. With the development of machine learning techniques, identification of abiotic stress and plant physiological changes from ChlF measurement without dark-adaption is desirable. The recent work on prediction of ChlF parameter Fv/Fm from ChlF measurement without dark-adaption shows promises of the

Table 6

Statistical analysis of wavelet entropy of rice ChlF under different drought levels excited by the PRBS signal. Values indicated with different letters in a row are significantly (p < 0.05) different from one another. The results are presented as means \pm standard errors values for n=120. I, II, III, and IV represent Hyou-518, Zhuliangyou-819, Xinliangyou-212, and Hanyou-2. Dd1, Dd2, and Dd3 refer to non-drought, drought stress for 3 days, and drought stress for 7 days, respectively. AEi and DEi represent the wavelet entropy of the ith (i=1,2,...6) approximation and detail components, respectively.

Varieties & Scales	Dd1	Dd2	Dd3	Varieties & Scales	Dd1	Dd2	Dd3
I-AE1	2.56 ±	2.66 ±	2.82 ±	I-AE2	2.55 ±	2.63 ±	2.79 ±
I-AE3	0.14c 2.56 ±	0.17b 2.66 ±	0.13a 2.80 ±	I-AE4	0.13c 2.61 ±	0.17b 2.71 ±	0.14a 2.85 ±
I-AE5	0.13c 2.61 ±	$\begin{array}{c} 0.17\mathrm{b} \\ 2.71 \\ \pm \end{array}$	0.13a 2.84 ±	I-AE6	0.13c 2.62 ±	0.16b 2.70 ±	0.13a 2.82 ±
I-DE1	0.13c 0.18 ±	0.16b 0.20 ±	$\begin{array}{c} 0.12a \\ 0.21 \\ \pm \end{array}$	I-DE2	0.11c 0.41 ±	0.14b 0.43 ±	0.11a 0.45 ±
I-DE3	0.01c 0.57 ±	0.01b 0.57 ±	0.01a 0.60 ±	I-DE4	0.03c 0.95 ±	0.03b 0.97 ±	0.02a 1.01 ±
I-DE5	0.08c 1.88 ±	0.04b 1.92 ±	0.05a 1.94 ±	I-DE6	0.05c 2.31 ±	0.04b 2.39 ±	0.07a 2.44 ±
II-AE1	0.09c 2.69 ±	0.07b 2.56 ±	0.08a 2.80 ±	II-AE2	0.09c 2.68 ±	0.09b 2.53 ±	0.07a 2.78 ±
II-AE3	0.14b 2.69 ±	0.24c 2.56 ±	0.14a 2.79 ±	II-AE4	0.14b 2.73 ±	0.24c 2.61 ±	0.15a 2.83 ±
II-AE5	0.14b 2.73 ±	0.23c 2.61 ±	0.14a 2.83 ±	II-AE6	0.14b 2.73 ±	0.22c 2.63 ±	0.14a 2.81 ±
II-DE1	0.14b 0.19 ±	0.21c 0.19 ±	0.14a 0.20 ±	II-DE2	0.12b 0.43 ±	0.18c 0.41 ±	0.12a 0.45 ±
II-DE3	0.01b 0.57 ±	0.01b 0.58 ±	0.01a 0.60 ±	II-DE4	0.03b 0.97 ±	0.04c 0.99 ±	0.03a 1.01 ±
II-DE5	0.03c 1.88 ±	0.05b 1.95 ±	0.04a 1.95 ±	II-DE6	0.05c 2.36 ±	0.06b 2.37 ±	0.06a 2.45 ±
III-AE1	0.07b 2.61 ±	0.07a 2.38 ±	0.06a 2.84 ±	III-AE2	0.08b 2.59 ±	0.10b 2.33 ±	0.06a 2.81 ±
III-AE3	0.16b 2.61	0.32c 2.39 ±	0.14a 2.83 ±	III-AE4	0.15b 2.65 ±	0.34c 2.44 ±	0.14a 2.87 ±
III-AE5	0.16b 2.65 ±	0.30c 2.47 ±	0.13a 2.87 ±	III-AE6	0.16b 2.66 ±	0.28c 2.52 ±	0.13a 2.85 ±
III-DE1	0.16b 0.19 ±	0.24c 0.19 ±	0.13a 0.21 ±	III-DE2	0.14b 0.42 ±	0.19c 0.41 ±	0.12a 0.46 ±
III-DE3	0.01b 0.58 ±	0.01b 0.60 ±	0.01a 0.58 ±	III-DE4	0.03b 0.98 ±	0.03b 1.03 ±	0.02a 1.01 ±
III-DE5	0.07b 1.92 ±	0.06a 2.00 ±	0.03a 1.92 ±	III-DE6	0.07b 2.36 ±		
IV-AE1	± 0.08b 2.53 ±	± 0.07a 2.43 ±	0.08b	IV-AE2	± 0.09b 2.53 ±	± 0.09b 2.41 ±	0.07a 2.60
IV-AE3	0.12b 2.53	0.24c 2.44 ±	0.26a 2.62 ±	IV-AE5	0.11b 2.57 ±	0.24c 2.50 ±	0.25a 2.67 ±
IV-AE5	0.12b 2.57 ±	0.22c 2.51 ±	0.25a 2.67 ±	IV-AE6	0.13b 2.59 ±	0.21c 2.55 ±	0.24a 2.67 ±
IV-DE1	± 0.13b 0.18 ±	0.19c 0.18 ±	± 0.22a 0.19 ±	IV-DE2	± 0.12b 0.40 ±	± 0.17b 0.40 ±	0.19a 0.43

Table 6 (continued)

Varieties & Scales	Dd1	Dd2	Dd3	Varieties & Scales	Dd1	Dd2	Dd3
IV-DE3	0.56 ± 0.05b 1.86 ± 0.10c	0.59 ± 0.06a 1.93 ± 0.09b	0.59 ± 0.06a 1.96 ± 0.09a	IV-DE4	0.95 ± 0.06c 2.29 ± 0.09c	0.98 ± 0.09b 2.33 ± 0.12b	1.00 ± 0.07a 2.39 ± 0.10a

machine learning-based methods (Xia et al., 2023). A prerequisite for machine learning techniques to be effective is that the training and testing data contain rich information, which is an advantage of the proposed broadband-based ChlF signals. For field measurement with a ChlF meter, switching between samples also takes a time for either a narrow-band or broadband excitation. Development of ChlF sensing networks to measure multiple samples at the same time can reduce measurement time

Sunlight-induced ChlF (SIF), a new vegetation remote sensing technology, has been developed rapidly in the past decade (Porcar-Castell et al., 2014). However, there is a gap between current SIF analysis and photosynthetic reactions. In reality, the SIF is induced by sunlight, which changes from the morning to the evening in intensity and is a broadband signal. Analysis of broadband-based ChlF signals through machine learning methods or mechanism-based models at the leaf or the canopy level will allow associating SIF at a large scale with photosynthetic reactions under natural light more directly. The rich photosynthetic reaction information carried by broadband-based ChlF will also allow extraction of photosynthetic rates and plant physiological status through either data-driven methods or mechanism-driven methods for various plant phenotype analysis and stress sensing. In the future, more research is needed to uncover the relationship between energy distribution difference in the frequency domain and photosynthetic electron transport rates or photosynthetic reactions.

6. Conclusion

In this work, the wavelet entropy of ChlF from PRBS excitation was used to differentiate samples under drought stress of different durations. While the features obtained from the OJIP-based ChlF features could not consistently differentiate the different groups under investigation, the wavelet entropy of PRBS-based ChlF differed significantly among different drought durations for multiple plant types and varieties. The results show that the wavelet entropy is a useful tool to analyze ChlF and PRBS is an alternative signal to perturb the system to produce ChlF with additional information. This work offers a new method to excite and analyze ChlF for plant abiotic stress sensing and plant phenomics characterization.

CRediT authorship contribution statement

Qian Xia: Methodology, Software, Writing – original draft, Writing – review & editing. Hao Tang: Investigation, Formal analysis. Lijiang Fu: Investigation, Formal analysis. Jinglu Tan: Formal analysis, Writing – review & editing. Ya Guo: Conceptualization, Methodology, Writing – review & editing, Supervision, Funding acquisition.

Declaration of Competing Interest

The authors declare that they have no known competing financial interests or personal relationships that could have appeared to influence the work reported in this paper.

Data availability

Data will be made available on request.

Acknowledgements

This project was partially supported by the National Natural Science Foundation of China (No: 51961125102, 31771680), Jiangsu Agricultural Science and Technology Innovataion Fund (SCX(22)3669), and the 111 Project (B23008).

References

- Akujuobi, C.M., 2022. Wavelets and Wavelet Transform Systems and Their Applications: A Digital Signal Processing Approach. Springer, Berno, Switzerland, pp. 55–80.
- Banks, J.M., 2018. Chlorophyll fluorescence as a tool to identify drought stress in Acer genotypes. Environ. Exp. Bot. 155, 118–127. https://doi.org/10.1016/j. envexpbot.2018.06.022.
- Barnabás, B., Jäger, K., Fehér, A., 2008. The effect of drought and heat stress on reproductive processes in cereals. Plant Cell Environ. 31 (1), 11–38. https://doi.org/ 10.1111/j.1365-3040.2007.01727.x.
- Chen, W., Jana, D., Singh, A., Jin, M., Cenedese, M., Kosova, G., Brake, M.R.W., Schwingshackl, C.W., Nagarajaiah, S., Moore, K.J., Noël, J.P., 2022. Measurement and identification of the nonlinear dynamics of a jointed structure using full-field data, Part I: Measurement of nonlinear dynamics. Mech. Syst. Signal Pr. 166, 108401 https://doi.org/10.1016/j.ymssp.2021.108401.
- Cruz, J.A., Savage, L.J., Zegarac, R., Hall, C.C., Satoh-Cruz, M., Davis, G.A., Kovac, W.K., Chen, J., Kramer, D.M., 2016. Dynamic environmental photosynthetic imaging reveals emergent phenotypes. Cell Syst. 2 (6), 365–377. https://doi.org/10.1016/j.cels.2016.06.001.
- Dąbrowski, P., Baczewska-Dąbrowska, A.H., Kalaji, H.M., Goltsev, V., Paunov, M., Rapacz, M., Wójcik-Jagła, M., Pawluśkiewicz, B., Bąba, W., Brestic, M., 2019. Exploration of chlorophyll a fluorescence and plant gas exchange parameters as indicators of drought tolerance in perennial ryegrass. Sensors 19 (12), 2736. https:// doi.org/10.3390/s19122736.
- Dąbrowski, P., Baczewska-Dąbrowska, A.H., Bussotti, F., Pollastrini, M., Piekut, K., Kowalik, W., Jacek, W., Kalaji, H.M., 2021. Photosynthetic efficiency of *Microcystis* ssp. Under salt stress. Environ. Exp. Bot. 186, 104459 https://doi.org/10.1016/j. envexpbot.2021.104459.
- Dietz, K.J., Zörb, C., Geilfus, C.M., 2021. Drought and crop yield. Plant Biol. 23 (6), 881–893. https://doi.org/10.1111/plb.13304.
- Ellerman, D., 2021. New foundations for information theory: logical entropy and Shannon entropy. Springer, New York, NY, USA.
- Eriksson, T.A., Bülow, H., Leven, A., 2017. Applying neural networks in optical communication systems: Possible pitfalls. IEEE Photonic. Tech. L. 29 (23), 2091–2094. https://doi.org/10.1109/lpt.2017.2755663.
- Esmaeilizadeh, M., Shamsabad, M.R.M., Roosta, H.R., Dąbrowski, P., Rapacz, M., Zieliński, A., Jacek, W., Kalaji, H.M., 2021. Manipulation of light spectrum can improve the performance of photosynthetic apparatus of strawberry plants growing under salt and alkalinity stress. PLoS One 16 (12), e0261585.
- Faseela, P., Sinisha, A.K., Brestič, M., Puthur, J.T., 2019. Chlorophyll a fluorescence parameters as indicators of a particular abiotic stress in rice. Photosynthetica 57 (SI), 108–115. https://doi.org/10.32615/ps.2019.147.
- Fiorani, F., Schurr, U., 2013. Future scenarios for plant phenotyping. Annu. Rev. Plant Biol. 64. 267–291. https://doi.org/10.1146/annurey-arplant-050312-120137.
- Gameiroa, C., Utkinbc, A.B., Cartaxanad, P., Marques da Silva, J., Matos, A.R., 2016. The use of laser induced chlorophyll fluorescence (LIF) as a fast and non-destructive method to investigate water deficit in Arabidopsis. Agr. Water Manage. 164 (1), 127–136. https://doi.org/10.1016/j.agwat.2015.09.008.
- Gerland, P., Raftery, A.E., Ševčíková, H., Li, N., Gu, D., Spoorenberg, T., Alkema, L., Fosdick, B.K., Chunn, J., Lalic, N., Bay, G., Buettner, T., Heilig, G.K., Wilmoth, J., 2014. World population stabilization unlikely this century. Science 346 (6206), 234–237. https://doi.org/10.1126/science.1257469.
- Gorbunov, M.Y., Falkowski, P.G., 2022. Using Chlorophyll Fluorescence to Determine the Fate of Photons Absorbed by Phytoplankton in the World's Oceans. Annu. Rev. Mar. Sci. 14, 213–238. https://doi.org/10.1146/annurev-marine-032621-122346.
- Guido, R.C., 2022. Wavelets behind the scenes: Practical aspects, insights, and perspectives. Phys. Rep. 985, 1–23. https://doi.org/10.1016/j.physrep.2022.08.001.
- Guo, Y., Tan, J., 2015a. Recent advances in the application of chlorophyll a fluorescence from photosystem II. Photochem. Photobiol. 91 (1), 1–14. https://doi.org/10.1111/ php.12362.
- Guo, Y., Zhou, Y., Tan, J., 2015b. Wavelet analysis of pulse-amplitude-modulated chlorophyll fluorescence for differentiation of plant samples. J. Theor. biol. 370, 116–120. https://doi.org/10.1016/j.jtbi.2015.01.041.
- He, Y., Xiao, Q., Bai, X., Zhou, L., Liu, F., Zhang, C., 2022. Recent progress of nondestructive techniques for fruits damage inspection: a review. Crit. Rev. Food Sci. 62 (20), 5476–5494. https://doi.org/10.1080/10408398.2021.1885342.
- Kalaji, H.M., Schansker, G., Ladle, R.J., Goltsev, V., Bosa, K., Allakhverdiev, S.I., Brestic, M., Bussotti, F., Calatayud, A., Dąbrowski, P., Elsheery, N.I., Ferroni, L., Guidi, L., Hogewoning, S.W., Jajoo, A., Misra, A.N., Nebauer, S.G., Pancaldi, S., Penella, C., Poli, D.B., Pollastrini, M., Romanowska-Duda, Z.B., Rutkowska, B., Serôdio, J., Suresh, K., Szulc, W., Tambussi, E., Yanniccari, M., Zivcak, M., 2014. Frequently asked questions about in vivo chlorophyll fluorescence: practical issues. Photosynth. Res. 122, 121–158. https://doi.org/10.1007/s11120-014-0024-6.
- Krause, G.H., Weis, E., 1991. Chlorophyll fluorescence and photosynthesis: the basics. Annu. Rev. Plant Biol. 42 (1), 313–349. https://doi.org/10.1146/annurev. arplant.42.1.313.

- Lazár, D., 2006. The polyphasic chlorophyll a fluorescence rise measured under high intensity of exciting light. Funct. Plant Biol. 33, 9–30. https://doi.org/10.1071/ fn05095
- Li, Z., Su, X., Chen, Y., Fan, X., He, L., Guo, J., Wang, Y., Yang, Q., 2021. Melatonin improves drought resistance in maize seedlings by enhancing the antioxidant system and regulating abscisic acid metabolism to maintain stomatal opening under PEG-induced drought. J. Plant Biol. 64 (4), 299–312. https://doi.org/10.1007/s12374-021.00297-3
- Liu, X., Pan, Y., Zhu, X., Yang, T., Bai, J., Sun, Z., 2018. Drought evolution and its impact on the crop yield in the North China Plain. J. Hydrol. 564, 984–996. https://doi.org/ 10.1016/j.jhydrol.2018.07.077.
- Lubitz, W., Reijerse, E.J., Messinger, J., 2008. Solar water-splitting into H₂ and O₂: design principles of Photosystem II and hydrogenases. Energ. Environ. Sci. 1 (1), 15–31. https://doi.org/10.1039/B808792J.
- Ma, J., Wang, J., Deng, K., Gao, Y., Xiao, W., Hou, J., Jiang, C., Jing, L.i., Yu, B., 2022. The effect of MaxiK channel on regulating the activation of NLRP3 inflammasome in rats of blast-induced traumatic brain injury. Neuroscience 482, 132–142. https://doi.org/10.1016/j.neuroscience.2021.12.019.
- Mahlein, A.K., Kuska, M.T., Behmann, J., Polder, G., Walter, A., 2018. Hyperspectral sensors and imaging technologies in phytopathology: State of the art. Annu. Rev. Phytopathol. 56 (1), 535–558. https://doi.org/10.1146/annurev-phyto-080417-050100.
- Mathobo, R., Marais, D., Steyn, J.M., 2017. The effect of drought stress on yield, leaf gaseous exchange and chlorophyll fluorescence of dry beans (*Phaseolus vulgaris* L.). Agr. Water Manage. 180, 118–125. https://doi.org/10.1016/j.agwat.2016.11.005.
- Mohammed, G.H., Colombo, R., Middleton, E.M., Rascher, U., van der Tol, C., Nedbal, L., Goulas, Y., Pérez-Priego, O., Damm, A., Meroni, M., Joiner, J., Cogliati, S., Verhoef, W., Malenovský, Z., Gastellu-Etchegorry, J., Miller, J.R., Guanter, L., Moreno, J., Moya, I., Berry, J.A., Frankenberg, C., Zarco-Tejada, P.J., 2019. Remote sensing of solar-induced chlorophyll fluorescence (SIF) in vegetation: 50 years of progress. Remote. Sens. Environ. 231, 111177 https://doi.org/10.1016/j. rse.2019.04.030.
- Murchie, E.H., Lawson, T., 2013. Chlorophyll fluorescence analysis: a guide to good practice and understanding some new applications. J. Exp. Bot. 64 (13), 3983–3998. https://doi.org/10.1093/jxb/ert208.
- Özbay, Y., Ceylan, R., Karlik, B., 2011. Integration of type-2 fuzzy clustering and wavelet transform in a neural network based ECG classifier. Expert. Sys. Appl. 38 (1), 1004–1010. https://doi.org/10.1016/j.eswa.2010.07.118.
- Pan, D., Dai, F., 2018. Design and analysis of a broadband vibratory energy harvester using bi-stable piezoelectric composite laminate. Energ. Convers. Manage. 169, 149–160. https://doi.org/10.1016/j.enconman.2018.05.032.
- Porcar-Castell, A., Tyystjärvi, E., Atherton, J., van der Tol, C., Flexas, J., Pfündel, E.E., Moreno, J., Frankenberg, C., Berry, J.A., 2014. Linking chlorophyll a fluorescence to photosynthesis for remote sensing applications: Mechanisms and challenges. J. Exp. Bot. 65 (15), 4065–4095. https://doi.org/10.1093/jxb/eru191.
- Qu, L., Li, L., Lee, J., 2003. Enhanced diagnostic certainty using information entropy theory. Adv. Eng. Inform. 17 (3–4), 141–150. https://doi.org/10.1016/j. aei.2004.08.002.
- Ruban, A.V., 2016. Nonphotochemical chlorophyll fluorescence quenching: mechanism and effectiveness in protecting plants from photodamage. Plant Physiol. 170 (4), 1903–1916. https://doi.org/10.1104/pp.15.01935.
- Simon, M.M., Greenaway, S., White, J.K., Fuchs, H., Gailus-Durner, V., Wells, S., Sorg, T., Wong, K., Bedu, E., Cartwright, E.J., Dacquin, R., Djebali, S., Estabel, J., Graw, J., Ingham, N.J., Jackson, I.J., Lengeling, A., Mandillo, S., Marvel, J., Meziane, H., Preitner, F., Puk, O., Roux, M., Adams, D.J., Atkins, S., Ayadi, A., Becker, L., Blake, A., Brooker, D., Cater, H., Champy, M., Combe, R., Danecek, P., Fenza, A.D., Gates, H., Gerdin, A., Golini, E., Hancock, J.M., Hans, W., Hölter, S.M., Hough, T., Jurdic, P., Keane, T.M., Morgan, H., Müller, W., Neff, F., Nicholson, G., Pasche, B., Roberson, L., Rozman, J., Sanderson, M., Santos, L., Selloum, M., Shannon, C., Southwell, A., Tocchini-Valentini, G.P., Vancollie, V.E., Westerberg, H., Wurst, W., Zi, M., Yalcin, B., Ramirez-Solis, R., Steel, K.P., Mallon, A., Angelis, M.H.D., Herault, Y., Brown, S.D.M., 2013. A comparative phenotypic and genomic analysis of C57BL/6J and C57BL/6N mouse strains. Genome Biol. 14 (7), 1–22. https://doi.org/10.1186/gb-2013-14-7-r82.
- Stirbet, A., Lazar, D., Kromdijk, J., Govindjee, G., 2018. Chlorophyll a fluorescence induction: can just a one-second measurement be used to quantify abiotic stress responses? Photosynthetica 56 (1), 86–104. https://doi.org/10.1007/s11099-018-0770-3.
- Sukhova, E., Sukhov, V., 2019. Analysis of light-induced changes in the photochemical reflectance index (PRI) in leaves of pea, wheat, and pumpkin using pulses of greenyellow measuring light. Remote Sens.-Basel 11 (7), 810. https://doi.org/10.3390/ rs11070810.
- Sukhova, E., Yudina, L., Gromova, E., Ryabkova, A., Kior, D., Sukhov, V., 2021. Complex analysis of the efficiency of difference reflectance indices on the basis of 400–700 nm wavelengths for revealing the influences of water shortage and heating on plant seedlings. Remote Sens-Basel 13 (5), 962. https://doi.org/10.3390/rs13050962.
- Sukhova, E., Kior, D., Kior, A., Yudina, L., Zolin, Y., Gromova, E., Sukhov, V., 2022a. New normalized difference reflectance indices for estimation of soil drought influence on pea and wheat. Remote Sens.-Basel 14 (7), 1731. https://doi.org/10.3390/ rs14071731.
- Sukhova, E., Yudina, L., Kior, A., Kior, D., Popova, A., Zolin, Y., Gromova, E., Sukhov, V., 2022b. Modified photochemical reflectance indices as new tool for revealing influence of drought and heat on pea and wheat plants. Plants 11 (10), 1308. https://doi.org/10.3390/plants11101308.
- Sun, Y., Wu, S., Zhang, J., Hwang, C., Yang, Z., 2020. Measurement Methodologies for Acoustic Noise Induced by Multilayer Ceramic Capacitors of Power Distribution

- Network in Mobile Systems. IEEE T. Electromagn. C. 62 (4), 1515–1523. https://doi.org/10.1109/TEMC.2020.2993850.
- Sundararajan, D., 2016. Discrete wavelet transform: a signal processing approach. John Wiley & Sons.
- Tribulato, A., Toscano, S., Lorenzo, V.D., Romano, D., 2019. Effects of water stress on gas exchange, water relations and leaf structure in two ornamental shrubs in the Mediterranean Area. Agronomy 9 (7), 381. https://doi.org/10.3390/agronomy9070381.
- Tsimilli-Michael, M., 2020. Revisiting JIP-test: An educative review on concepts, assumptions, approximations, definitions and terminology. Photosynthetica 58 (SI), 275–292. https://doi.org/10.32615/ps.2019.150.
- Wang, G., Liao, W.H., Zhao, Z., Tan, J., Cui, S., Wu, H., Wang, W., 2019. Nonlinear magnetic force and dynamic characteristics of a tri-stable piezoelectric energy harvester. Nonlinear Dynam. 97 (4), 2371–2397. https://doi.org/10.1007/s11071-019-05133-z.
- Wang, Y., Zhang, B., Jiang, D., Chen, G., 2018. Silicon improves photosynthetic performance by optimizing thylakoid membrane protein components in rice under drought stress. Environ. Exp. Bot. 158, 117–124. https://doi.org/10.1016/j. envexpbot.2018.11.022.
- Wang, D., Zhong, J., Shen, C., Pan, E., Peng, Z., Li, C., 2021. Correlation dimension and approximate entropy for machine condition monitoring: Revisited. Mech. Sys. Signal Pr. 152, 107497 https://doi.org/10.1016/j.ymssp.2020.107497.
- Wangpraseurt, D., Lichtenberg, M., Jacques, S.L., Larkum, A.W., Kühl, M., 2019. Optical properties of corals distort variable chlorophyll fluorescence measurements. Plant Physiol. 179 (4), 1608–1619. https://doi.org/10.1104/pp.18.01275.
- Webber, H., Ewert, F., Olesen, J.E., Müller, C., Fronzek, S., Ruane, A.C., Bourgault, M., Martre, P., Ababaei, B., Bindi, M., Ferrise, R., Finger, R., Fodor, N., Gabaldón-Leal, C., Gaiser, T., Jabloun, M., Kersebaum, K., Lizaso, J.I., Lorite, I.J., Manceau, L., Moriondo, M., Nendel, C., Rodríguez, A., Ruiz-Ramos, M., Semenov, M.A., Siebert, S., Stella, T., Stratonovitch, P., Trombi, G., Wallach, D., 2018. Diverging importance of drought stress for maize and winter wheat in Europe. Nat. Commun. 9 (1), 4249. https://doi.org/10.1038/s41467-018-06525-2.

- Wols, B.A., Hofman-Caris, C.H.M., 2012. Review of photochemical reaction constants of organic micropollutants required for UV advanced oxidation processes in water. Water Res. 46 (9), 2815–2827. https://doi.org/10.1016/j.watres.2012.03.036.
- Wu, F.Z., Bao, W.K., Li, F.L., Wu, N., 2008. Effects of drought stress and N supply on the growth, biomass partitioning and water-use efficiency of Sophora davidii seedlings. Environ. Exp. Bot. 63 (1–3), 248–255. https://doi.org/10.1016/j.envexplot.2007.11.002
- Xia, Q., Fu, L.J., Tang, H., Song, L., Tan, J.L., Guo, Y., 2022. Sensing and classification of rice (Oryza sativa L.) drought stress levels based on chlorophyll fluorescence. Photosynthetica 60 (1), 102–109. https://doi.org/10.32615/ps.2022.005.
- Xia, Q., Tang, H., Fu, L., Tan, J., Govindjee, G., Guo, Y., 2023. Determination of Fv/Fm from Chlorophyll a Fluorescence without Dark Adaptation by an LSSVM Model. Plant Phenomics 5, 0034. https://doi.org/10.34133/plantphenomics.0034.
- Xiao, M., Li, Y., Wang, J., Hu, X., Wang, L., Miao, Z., 2019. Study on the Law of Nitrogen Transfer and Conversion and Use of Fertilizer Nitrogen in Paddy Fields under Water-Saving Irrigation Mode. Water 11 (2), 218. https://doi.org/10.3390/w11020218.
- Xu, Q., Ma, X., Lv, T., M.B., Wang, Z., Niu J., 2020. Effects of Water Stress on Fluorescence Parameters and Photosynthetic Characteristics of Drip Irrigation in Rice. Water 12(1), 289. Doi:10.3390/w12010289.
- Yang, J., Shao, H., Ma, Y., Wan, L., Zhang, Y., Jiang, J., Du, J., Tang, G., 2020. Quantitative ultrashort echo time magnetization transfer (UTE-MT) for diagnosis of early cartilage degeneration: comparison with UTE-T2* and T2 mapping. Quant. Imag. Med. Surg. 10 (1), 171–183. https://doi.org/10.21037/qims.2019.12.04.
- Yao, J., Sun, D., Cen, H., Xu, H., Weng, H., Yuan, F., He, Y., 2018. Phenotyping of Arabidopsis drought stress response using kinetic chlorophyll fluorescence and multicolor fluorescence imaging. Front. Plant Sci. 9, 603. https://doi.org/10.3389/ fpls.2018.00603.
- Zhuang, J., Wang, Y., Chi, Y., Zhou, L., Chen, J., Zhou, W., Song, J., Zhao, N., Ding, J., 2020. Drought stress strengthens the link between chlorophyll fluorescence parameters and photosynthetic traits. PeerJ 8, e10046.